POLITECNICO
MILANO 1863

SCUOLA DI INGEGNERIA INDUSTRIALE
E DELL'INFORMAZIONE

Analysis of the performance of an ultra-wide band localization system using Bayesian tracking filters

Tesi di Laurea Magistrale in
Telecommunication Engineering - Ingegneria delle
telecomunicazioni

Author: **Luca De Angelis**

Student ID: 000000
Advisor: Prof. Monica Barbara Nicoli
Co-advisors: Marco Piavanini, Luca Barbieri
Academic Year: 2021-22

Abstract

Ultra-Wide Band (UWB) technology has reached incredible performance and precision in short range indoor localization. The problem of reaching a good positioning also for moving targets with a very high precision is incredible challenging even today, more so when considering highly cluttered or closeted environments. A moving target needs to be described in the most optimal way to achieve a good tracking solution and the usage of inertial sensors (IMU), advanced motion modeling and Bayesian tracking algorithm is fundamental to reach good enough performances. The goal of this thesis is to provide an understanding of the challenges and the solution of a moving target, considering all the difficulties an UWB system can find working in an indoor environment. The implementation of a well designed filter, such as the Extended Kalman Filter (EKF) for a tracking solution is essential to meet the goal of improving an already integrated system designed to be "plug-and-play", with the aim of being used in many different environment to track a good variety of targets. The utilization in sport applications can be different from more office-based scenario, where the moving target is more stiff, or may even be an automated small vehicle used for logistics. For this purpose the usage of a variety of motion models adapted to the amount of information available is crucial to reach a good enough positioning error with respect to the actual true path. In the following work an analysis of the experimental results performed using an UWB localization system based on ranging methods such as TOA (Time of arrival) and TDoA (Time difference of arrival) are performed. The results are shown using a Bayesian Extended Kalman filter, comparing the performances with different localization methods, such as an LS (Least Square) algorithm and the pre-elaborated positions provided by the system itself, as well as the comparison of the solutions provided using different motion models and comparing the system's performances with the auto-localization algorithm for the anchors position.

Abstract in lingua italiana

La tecnologia Ultra-Wide Band (UWB) ha raggiunto performance di incredibile precisione per applicazioni in ambito di localizzazione indoor per situazioni riguardanti il corto raggio. Raggiungere una certa precisione anche nella localizzazione di obiettivi in movimento è incredibilmente difficile anche al giodno d'oggi, ancor più se si considerano nell'equazione la presenza di ambienti chiusi o molto ricchi di ostacoli. Un oggetto in movimento deve essere descritto nella maniera più ottimale per raggiungere una soluzione soddisfacente a livello di tracking. A questo scopo l'utilizzo di sensori inerziali (IMU), modelli di moto avanzati o algoritmi per l'implementazione di filtri Bayesiani è fondamentale se si vuole raggiungere delle performance sufficientemente alte. L'obiettivo di questa tesi è quello di fornire una visione su quelle che sono le difficoltà e le soluzioni dell'avere un target in movimento da localizzare, prendendo in atto tutte le difficoltà che un sistema UWB può presentare lavorando in un ambiente indoor. Implementare un filtro adeguatamente calibrato, come l'Extended Kalman filter, è essenziale se si vuole migliorare un sistema designato per l'applicazione "plug-and-play", con funzione principale quella di essere utilizzato in ambienti molto diversi, con la possibilità di dover poter localizzare una varietà molto estesa di obiettivi. L'implementazione può variare molto se si considera un'applicazione di tipo sportivo, piuttosto che quella relativa ad un ambienta simile ad un ufficio od una fabbrica, dove possiamo trovare andature più moderate nelle persone o addirittura possibili applicazioni su veicoli automatizzati a fini logistici in ambienti industriali. Per questo motivo, l'utilizzo di diversi modelli di moto deve essere adattato alla quantità di informazioni in proprio possesso per minimizzare l'errore di posizione rispetto al percorso realmente effettuato. In questo elaborato è effettuata un'analisi sperimentale delle performance di un sistema di localizzazione UWB basato su metodi di misurazione della distanza come TOA (Time of arrival) o TDoA (Time difference of arrival. I risultati sono mostrati con l'utilizzo di un Extended Kalman filter (EKF), performando diversi paragoni con altri metodi di localizzazione, come un algoritmo LS (Least square) e l'utilizzo dei dati pre-elaborati dal sistema di localizzazione UWB preso in considerazione. Oltre a questo, sono mostrati anche i dati ricavati dal paragone generato dall'utilizzo di diversi modelli di moto e dal confronto con l'algoritmo di auto-localizzazione delle ancore già presente

nel sistema di riferimento.

Contents

1 | Introduction

The usage of Ultra Wide-Band (UWB) frequencies for localization applications outside of military purposes started to be increased twenty years ago. The higher frequency range was optimal to be utilized in many indoor scenarios. Since then, the number of fields in which this technology could spread have become numerous: from medical, security, road and driving management, automotive and even sportive applications have been deployed.[11]

Although UWB systems can achieve nowadays high accuracy there are several restrictions concerning the output power emitted by the system, reducing its spectral mask and enabling the devices to be mostly used for short-range wireless positioning. For the sake of positioning, several ranging methods are commonly used: Based on power signal loss, a Received Signal Strength (RSS) solution is applicable; Time based techniques, such as Time-of-Arrival (ToA), requiring clock synchronization between the used nodes of the system, or Time-Difference of Arrival (TDoA) which can resolve the problem of clock synchronization.[19]

Indoor positioning is a very challenging task to achieve, therefore, many methods have been tested. RSS based techniques combined with fingerprinting is very largely utilized [18], but usually the position can also be estimated trough the addition of previous position estimate and position displacement from sensor-based techniques using the help of adaptive algorithms, such as Kalman filters. [17] In indoor environments, despite the use of detection strategies, the pseudo-range estimate can be biased from actual distances. This usually happens in case of blockage situations or when it is not possible to estimate a definite geometrical path trough the localization process. Adding to this, when trying to localize a moving target in a closeted environment, the difficulty increases drastically. Bayesian filtering is so a fitting solution, inserting a statistical approach to the problem. Defining the driving process of movement of the target is fundamental and matching its statistical representation with the actual information obtainable from the devices, such as velocity or acceleration data from inertial sensors, can increase the probability of actually performing an accurate positioning. [2]

1.1.   State of the art

The process of indoor positioning of a moving target is not an easy riddle to solve. Considering the case in which a localization system is deployed with a set of anchors, defined as the radiating devices used for the reference system, and a set of tags, used to send information about its positioning, several techniques were deployed in literature. Considering the case of ranging measurements, it is possible to deploy filtering solutions such as particle filters(PF), using a weighted set of particles to estimate the position of the target [10], and even combine the latter with map-based techniques to obtain a high accuracy in very complex environment using pre-existent data. [14] The use of maps is also used to filter the environment itself, designing specific areas to singular actions or target behaviour to integrate in potential predictive algorithms.[15] Bayesian filters also provides several solutions to the problem. The Kalman filter (KF), and its evolution for the application on non-linear situations: Extended Kalman filter (EKF) is vastly used in the literature, such as: [17], [4] and [3]. A less computationally complicated tracking filter characterized by a large usage in the field is the Unscented Kalman filter (UKF), which provides a carefully selected set of points (sigma points) to predict the position of the target in the current state. [20] [21]

Combining the previously mentioned techniques with many different technologies is crucial for the implementation of innovative solutions. The fusion of IOT (Internet of Things) technology and more advanced sensors and inertial units, are enabling the possibility to track with more precision human targets in walking, running and other types of motion. The study of the human gait [22] and the actual movements of the person's limbs [13] are opening the possibilities to the usage of mixed motion models [8] beyond the classical "random walk", including heading-based models, inverted pendulum, and acceleration based models to monitor the step length and frequency aiming to achieve higher accuracy in the complicated task of people localization.

1.2.   Thesis contribution and outline

The objective of this thesis is to test the UWB devices provided by Tracking 4 Fun (T4F) and verify the system's performance in different scenarios. The main focus is the indoor application, where several experiments were made in an environment simulating an office-like or industrial scenario, in order to test the system's performance in a highly disturbed and cluttered situation. In addition to the testing phase, the project required the implementation of a tracking filter (Extended Kalman filter) to improve the performance of the

devices and the pre-functioning algorithm already integrated into the system. The algorithm was tested in comparison to different outcomes (such as an LS algorithm and the raw data extrapolated from the T4F application), comparing different motion models and testing the reliability of the anchor's auto-localization algorithm. An outdoor experiment was also conducted, the results are in fact reported.

The Thesis is structured in the following way:

- **Chapter 2**: Overview of the main advantages and disadvantages of the UWB technology, describing the main causes of losses in the application in indoor environment comparing with the outdoor counterpart.

- **Chapter 3**: Describes the main solutions regarding the localization of a moving target, focusing on the main motion models used in the tracking procedure, highlighting the most suited for the human walking movement. An overview on the functioning of the Bayesian filters is also provided, describing the equations and mathematics behind the Kalman filter solution.

- **Chapter 4**: This chapter describes the experimental campaign. The T4F devices and the different scenarios are illustrated as well as the challenges and solutions for the data processing of the TDoA results and the preparation for the filtering phase.

- **Chapter 5**: In this chapter all of the experimental results are illustrated. Providing a full insight on the differences on the performance of the devices in the various scenarios. Path comparison, positioning error estimation and visual representation of the tracking process are discussed as well as the analysis of different motion models and anchor position differences.

2 | Ultra-wide band localization system

This chapter introduces the characteristics of the Ultra-wide Band (UWB) system developed by Tracking 4 Fun (T4F) used in the experimental campaigns. The main features of the Ultra-wide band devices are described considering a general use case scenario and subsequently the challenges and the main problems of indoor and outdoor applications are introduced. Both applications are discussed, providing a full understanding of the factors in play during the two different campaigns. The problems and the possible solutions are illustrated in order to have a clear picture of how the devices operates and can overcome some of the difficulties of the real-life application.

UWB signals are characterized by a very large bandwidth which provides useful characteristics for positioning purposes. First of all, this kind of technology can achieve a large time resolution and facilitates a more accurate range estimation and, therefore, an accurate position in the localization scenario. UWB signals also provide a high-speed data transmission and a very large frequency range available. In addition to this, it is possible to achieve high enough frequencies to penetrate trough obstacles. The very good performances in the ranging process makes UWB systems well suited for short-range wireless sensor networks (WSNs) enabling applications in many different fields, such as security, military, biomedical and industrial scenarios, adapting sufficiently well in both indoor and outdoor environments [7].

2.1. Challenges and solutions of UWB systems

In a typical outdoor situation, the position information of a user can be easily extracted using satellite systems such as GPS (Global Positioning System) or Galileo (European satellite navigation system). These systems can reach a very good accuracy in open space scenarios, where the signal is not affected by the interruption of the connection caused by the cluttering of urban environments and high multi-path and losses related to the presence of buildings and closed areas. In those cases adopting different solution

integrating the UWB technology is crucial to achieve acceptable performance results.

In the UWB wireless positioning technology, the location is calculated using the Time of Flight (TOF) between the transmitter point and the receiver. The main problem appears when the communication condition is not in the Line-of-Sight condition anymore. This situation is verified only when the signal is not obscured by any obstacle between transmitter and receiver. In that case, an entirely different framework installed inside the offices, homes and buildings may be needed to compensate the difficulties of the communication on the current infrastructure. Additional antennas and indoor wireless networks can help mitigate the problem [16].

The following paragraphs illustrate the main cause of uncertainty in indoor environments, describing the case of a moving target and how to combine different techniques to obtain more accurate positioning results.

2.1.1. Outdoor vs indoor localization

The UWB technology uses as its main principle the transmission of ultra-short pulses (less than 1ns) signals over multiple frequencies. This Technology can guarantee a localization accuracy of the order of centimetres. This solution, which allows the system to access a very large bandwidth, is not only a low-cost innovation in terms of energy consumption, but it also facilitates the elaboration of the signal in the case of multiple channels and NLoS (Non-Line of Sight) scenarios.

A radio signal transmitted from a fixed source in a typical urban or indoor environment will encounter multiple obstacles producing different reflected, diffracted or scattered copies of the transmitted signal. Those copies are called multi-path signal components which are usually attenuated in terms of power, delayed in time and shifted in frequency or phase from the LOS (Line of Sight) path at the receiver. Taking into account the case of an indoor environment, there are many factors influencing the attenuation. The layout of the rooms, the different materials used for walls, floors, windows, the material and location of obstructing objects, as well as the very size of the rooms.

Generalizing the case scenario, it is possible to describe a simplified model for path-loss as a function of distance:

$$P_r = P_t * K[\frac{d}{d_0}] \tag{2.1}$$

We can write the dB attenuation as:

$$P_{rdBm} = P_{tdBm} + K_{dB} - 10\gamma log_{10}[\frac{d}{d_0}] \tag{2.2}$$

Where K is a constant depending on the antenna characteristics and the channel attenuation in average, d_0 is the reference distance for the antenna far-field, and γ is the path-loss exponent. This kind of model is valid for distances $d > d_0$ with d_0 assumed 1-10 m in indoor scenarios and up to 100 m in outdoor environments.[5]

2.1.2. Multi-path Fading

Blockage from other objects is also a determining factor on affecting the received signal. This phenomenon will give rise to random variations of the received power at a given distance. The cause of such variations can be found in changes in reflecting surfaces and scattering objects causing a consequential attenuation of the overall signal. The attenuation phenomena is related to the material composition and dielectric properties of the objects obstructing the signal which alters the reflection of the signal hitting the scattering surfaces. The attenuation generated by these are unknown and some statistical models are used to describe the situation in both indoor and outdoor situations.

The wireless signal transmitted experiences random variations during the propagation when objects block the signal path. In a typical indoor or urban environment, a radio signal will encounter multiple obstacles and objects that can produce reflected, diffracted or scattered copies of the transmitted signal all of which will be composing the multi-path components. Those components can appear: attenuated in power, shifted in phase or frequency from the LOS path and delayed in time. It is possible to model these fluctuations in the signal as a log-normal, which mean that it can be approximated as a

		Parameters				
		Accuracy[m]	Coverage [m]	Cost	Complexity	Typical Environment
Technologies	Vision	$10^{-3} \div 10^{-1}$	1-10	High	High	Indoor
	Infrared	$10^{-2} \div 1$	1-5	Medium/High	Low	Indoor
	Ultrasound	10^{-2}	2-10	Medium	Low	Indoor
	Wi-Fi	$1 \div 10$	20-50	Medium/Low	Low	Indoor/Outdoor
	RFID	$10^{-1} \div 1$	1-10	Low	Low	Indoor
	Bluetooth	$1 \div 10$	1-30	Low	Low	Indoor/Outdoor

Figure 2.1: Table describing the different characteristics of a series of technologies used for indoor positioning.[12]

Gaussian distributed variable logarithmic scale Gaussian distributed variable.

$$\frac{1}{x\sigma\sqrt{2\pi}}exp(-\frac{(ln(x)-\mu)^2}{2\sigma^2}) \tag{2.3}$$

with μ as the mean and σ the standard deviation. Thus the path loss equation can be rewritten as:

$$P_{rdBm} = P_{rdBm} + S \tag{2.4}$$

$$S \, \mathcal{N}(0, \sigma_{dB}^2) \tag{2.5}$$

The Shadowing effect is usually characterized by a standard deviation between 3 and 5 dB. Given that the UWB signal experiences a very short pulse periods, it is possible to use a 3dB standard deviation for the log-normal fading.

Considering the situation of a very cluttered scenario with the presence of a clear multi-path, we can observe the effect of the delay spread $\Delta\tau$ characterizing the broadening of the pulse duration which have been demonstrated to be equal to the inverse of the bandwidth and, thus, will have different effects depending on the bandwidth itself. Taking into account the last sentence, it is possible to deduce that, given the very high bandwidth of the UWB systems, the multi-path fading effect is very much mitigated as the delay spread is very little since the extremely large bandwidth [5].

3 | Localization of moving targets

This chapter describes the main problems and techniques used to characterize the dynamics of a moving target, in particular pedestrians, in a localization system. The problem of realistically describing the human body and its movements has been studied for many years. Nowadays there are several models to virtually simulate the gait of a person in several situations. The step detection, step length, gait estimation, human heading, velocity estimation and many more characteristics have been examined to describe in the best way possible the evolution of a person's path in a variety of situations.

The localization of a moving target is not an easy task, the techniques needs to include the update of the estimate of the target over time, as well as the use of Bayesian filters with the employment of different motion models needs to be considered. The more information is available about the moving target, the more the localization accuracy can increase, leading to a more precise positioning results. The experiments conducted with the T4F system were suited for walking and running targets, therefore it is important to understand the main differences in the positioning of the tags on the subject's body in order to have a better understanding on how to improve the localization accuracy knowing the main features of the walking action. It is also important to understand the main differences in the application of a variety of motion models depending on the dynamics of the system in consideration.

3.1. Motion models for human tracking

To fulfil the goal of achieving a good localization accuracy and to obtain a good prediction in the tracking of a moving target it is important to use the information we get from the sensors we have and the observations of the target's state. To do this we need to describe an optimal motion model to reflect the target's movement and obtain, combining it with the measurements related to the technology used, a better prediction of the moving tag.

To ensure an effective model-based approach, a mathematical representation of the model

needs to be used. It is possible to generalize the model using the following equations:

$$x_{k+1} = f_k(x_k, u_k, w_k) \tag{3.1}$$

$$z_k = h_k(x_k) + v_k \tag{3.2}$$

Where x_k, z_k and u_k are, respectively, the target state, observation and control input vectors at the discrete time t_k; w_k and v_k are process and measurement noise, while f_k and h_k are some vector-valued time-varying functions.

The general equation can be easily used to describe a motion model, since the tracking may lack the knowledge of the actual control input u of the target, the actual form of f, or the statistical properties of the noise w. Thus, describing a model that can provide the information we need given a pre-decided input is the base of the tracking process.

In the next sections several motion models are described for the human walking and running event along with the main characteristics of the most commonly used generalizations to use these models in an adaptive filtering algorithm.

3.1.1.   Random walk model

Considering what the most accurate motion models for human walk are, it is possible to do several generalizations: First of all, we utilize first-order Markov models which predicts that the state of an entity at a particular position in a sequence depends only on the state of the same entity at the preceding position. This premise permits to model the system in a way to only have to consider the prior measurement to be able to predict the current one.

Considering the complexity of the human walking process, it is possible to adopt the simplest solution, using then a Random Walk model, which is characterized in the following way:

$$x_t = u_t = \begin{bmatrix} u_{x,t} \\ u_{y,t} \end{bmatrix} \tag{3.3}$$

$$\begin{cases} u_{x,t} = u_{x,t-1} + Tw_{vx,t-1} & \text{(3.4a)} \\ u_{y,t} = u_{y,t-1} + Tw_{vy,t-1} & \text{(3.4b)} \end{cases}$$

where $w_{v,t-1}$ is the driving process defined as a random velocity process

$$w_{v,t-1} = \frac{u_t - u_{t-1}}{T} \tag{3.5}$$

it is possible to generalize the equations describing the model as:

$$u_t = u_{t-1} + T w_{v,t-1} \tag{3.6}$$

The probability of position transition $u_{t-1} \to u_t$ depends on the statistics of $w_{v,t}$:

$$p(u_t|u_{t-1}) = p_w(\frac{u_t - u_{t-1}}{T}) \tag{3.7}$$

The driving process is a random velocity process using the velocity as a Gaussian distributed random variable with zero-mean and standard deviation σ_v, so the position at time t is Gaussian distributed around the position at time t-1 with standard deviation $\sigma_v T$ [8]

$$w_{v,t} \, \mathcal{N}(0, \sigma_v^2 \mathbf{I}_2) \to u_t \, \mathcal{N}(u_{t-1}, (T\sigma_v)^2 \mathbf{I}_2) \tag{3.8}$$

3.1.2.   Random force model

Having more information provided by an IMU sensor enables the development of more complicated models, for example we can have a velocity sensor model, providing information about the velocity measured (for instance, by a speedometer in a car). In this case the zero-mean driving noise is the position variations given the velocity measured. The equations (3.4a) and (3.4b) become:

$$\begin{cases} u_{x,t} = u_{x,t-1} + T(v_{x,t-1} + w_{vx,t-1}) & (3.9a) \\ u_{y,t} = u_{y,t-1} + T(v_{y,t-1} + w_{vy,t-1}) & (3.9b) \end{cases}$$

with:

$$v_t = \begin{bmatrix} v_{x,t} \\ v_{y,t} \end{bmatrix} \tag{3.10}$$

we can see that the mean velocity is deterministic, while $w_{vx,t-1}$ and $w_{vy,t-1}$ are the zero-mean driving noise modeling the position variations, described as:

$$w_{vt} \, \mathcal{N}(0, \sigma_v^2 \mathbf{I}_2) \to u_t \, \mathcal{N}(u_{t-1} + Tv_{t-1}, (T\sigma_v)^2 \mathbf{I}_2) \tag{3.11}$$

If the velocity is included in the unknown vector and estimated together with the position, a random walk model is assumed for the velocity while the position is obtained integrating the velocity itself. In this case we have a Random Force model assuming the velocity as constant and the acceleration as a random driving process. We thus have a zero-mean Gaussian distribution for the acceleration.

$$
\begin{cases}
u_{x,t} = u_{x,t-1} + Tv_{x,t-1} + \dfrac{T^2}{2}w_{ax,t-1} & \text{(3.12a)} \\[2mm]
u_{y,t} = u_{y,t-1} + Tv_{y,t-1} + \dfrac{T^2}{2}w_{ay,t-1} & \text{(3.12b)} \\[2mm]
v_{x,t} = v_{x,t-1} + Tw_{ax,t-1} & \text{(3.12c)} \\[2mm]
v_{y,t} = v_{y,t-1} + Tw_{ay,t-1} & \text{(3.12d)}
\end{cases}
$$

where:

$$
w_{a,t} = \begin{bmatrix} v_{ax,t} \\ v_{ay,t} \end{bmatrix} = \frac{v_t - v_{t-1}}{T} \tag{3.13}
$$

The velocity is included into the unknown vector and estimated together with the position.

$$
\begin{bmatrix} u_{x,t} \\ u_{y,t} \\ v_{x,t} \\ v_{y,t} \end{bmatrix} =
\begin{bmatrix} 1 & 0 & T & 0 \\ 0 & 1 & 0 & T \\ 0 & 0 & 1 & 0 \\ 0 & 0 & 0 & 1 \end{bmatrix}
\begin{bmatrix} u_{x,t-1} \\ u_{y,t-1} \\ v_{x,t-1} \\ v_{y,t-1} \end{bmatrix} +
\begin{bmatrix} \frac{T^2}{2} & 0 \\ 0 & \frac{T^2}{2} \\ T & 0 \\ 0 & T \end{bmatrix}
\begin{bmatrix} w_{vx,t-1} \\ w_{vy,t-1} \end{bmatrix} \tag{3.14}
$$

That can be written in a closed form as:

$$
\mathbf{x_t} = \mathbf{F}\mathbf{x}_{t-1} + \mathbf{L}\mathbf{w}_{a,t-1} \tag{3.15}
$$

with zero-mean Gaussian acceleration:

$$
w_{a,t}\ \mathcal{N}(0, \sigma_a^2 \mathbf{I_2}) \rightarrow x_t\ \mathcal{N}(\mathbf{F}\mathbf{x}_{t-1}, \sigma_a^2 \mathbf{L}\mathbf{L}^T) \tag{3.16}
$$

is the driving process, described as a random acceleration process. These are the most common models to describe a walking person's gait, but the problem is a more complicated one, since the human walk is subjected to much more random variations of velocity and heading. The Random Force model can be adopted, but is more likely to be effective if the subject is in fact a vehicle or if the person is actually doing a specific activity such as jogging or running which can provide a higher probability of having a constant velocity [8].

3.1.3. Random jerk model

In the process of acquiring information from the human movement, providing data from an accelerometer or a gyroscope it is possible to describe much more complicated models including the acceleration as the known factor. In this case, integrating two times it is possible to obtain to the position of the target. [13]

For what concern the constant-acceleration model we can talk about a Random Jerk model which can be described using the acceleration as a white noise process $w(t) = \dot{a}(t)$. The corresponding state-space representation is:

$$\dot{x}(t) = \begin{bmatrix} 0 & 1 & 0 \\ 0 & 0 & 1 \\ 0 & 0 & 0 \end{bmatrix} x(t) + \begin{bmatrix} 0 \\ 0 \\ 1 \end{bmatrix} w(t) \tag{3.17}$$

which we can write as discrete-time equivalent as:

$$x_{k+1} = F_3 x_k + w_k \tag{3.18}$$

with:

$$F_3 = \begin{bmatrix} 1 & T & \frac{T^2}{2} \\ 0 & 1 & T \\ 0 & 0 & 1 \end{bmatrix} \tag{3.19}$$

We can write the state equation of the jerk model as:

$$\begin{bmatrix} x \\ \dot{x} \\ \ddot{x} \\ \dddot{x} \end{bmatrix} = \begin{bmatrix} 0 & 1 & 0 & 0 \\ 0 & 0 & 1 & 0 \\ 0 & 0 & 0 & 1 \\ 0 & 0 & 0 & -\alpha \end{bmatrix} \begin{bmatrix} x \\ \dot{x} \\ \ddot{x} \\ \dddot{x} \end{bmatrix} + \begin{bmatrix} 0 \\ 0 \\ 0 \\ 1 \end{bmatrix} w_t \tag{3.20}$$

where $x, \dot{x}, \ddot{x}, \dddot{x}$ are respectively the position, velocity, acceleration and jerk of the target and α is the reciprocal of the jerk time constant.

3.2. Algorithms for the localization of a moving target

Based on the acquisitions we want to take into consideration in this thesis, it is important to describe what are the means used to estimate the position from the provided measure-

ments. The main tool used are Bayesian filters, in particular, Extended Kalman Filter (EKF). The need to use this kind of filter is related to the necessity to use the information assumed by the motion model into the estimation of the current position.

3.2.1. Bayesian filters

Bayesian filters probabilistically estimate a dynamic system's state from noisy observations. Bayes filters represent the state at time t by random variables x_t, at each point in time. The aim is to sequentially estimate a belief (or guess) over the state space conditioned on all information contained in the sensor's data.

The goal is to understand what is the probability that the target we want to locate is in a specific location given the history of a specific sensor measurement. Usually this calculation can be very complex and the estimation of the posterior probability can be harder over time as the number of sensors measurements increases. For this reason, we assume the dynamic system as Markovian, so that the current state variable x_t contains all the relevant information given the fact that only the t-1 measurement is taken into consideration. To update a Bayes filter whenever a sensor provides a new observation z_t, the filter predicts the state according to:

$$Bel(x_t) = \int p(x_t|x_{t-1})Bel(x_{t-1})dx_{t-1} \tag{3.21}$$

The filter then corrects the predicted estimate using the sensor observation. $p(x_t|x_{t-1})$ describes the system dynamics, thus providing information of how the system's state changes over time. This model strongly depends on the information available to the estimation process [4]. This kind of filters are a good probabilistic framework for recursive state estimation.

The Bayesian tracking process requires the definition of two models: the system motion model for the evolution of the target and the measurement model relating the localization measurements to the current position. We obtain respectively two equations:

$$x_t = f_t(x_{t-1}, w_t) \tag{3.22}$$

$$y_t = h_t(x_t, n_t) \tag{3.23}$$

with $f_t(.)and h_t(.)$ described as deterministic time-varying functions, w_t the driving process noise and n_t the measurement noise. With the Bayes rule, we can write the posterior pdf

as:

$$p(x_t|y_{1:t}) = \frac{p(y_t|x_t)p(x_t|y_{1:t-1})}{p(y_t|y_{t-1})} = \Gamma p(y_t|x_t)p(x_t|y_{1:t-1}) \qquad (3.24)$$

With $p(y_t|x_t)$ is the likelihood pdf and $p(x_t|y_{1:t-1})$ defined as the prior pdf. Γ is a scaling factor. The current position is estimated trough the tracking process of defininf a prediction step and an update step:

- **Prediction**: The prior probability is computed using the posterior one at time t-1, the probability $p(x_{t-1}|y_{1:t-1})$ and the transition probability $p(x_t|x_{t-1})$ using the Chapman-Kolomogorov equation:

$$p(x_t|y_{1:t-1}) = \int p(x_t|x_{t-1})p(x_{t-1}|y_{1:t-1})\, dx_{t-1} \qquad (3.25)$$

- **Update**: the posterior pdf $p(x_t|y_{1:t})$ is computed trough the prior calculated during the update step and the use of the likelihood pdf. Trough this passage we can obtain a Maximum a Posteriori (MAP) estimatoe or a Minimum Mean Square Error (MMSE), described respectively as:

$$\hat{x}_{MAP} = argmax_x p(x|y_{1:t}) \qquad (3.26)$$

$$\hat{x}_{MMSE} = argmin_x E||x - \hat{x}||^2 = \int x p(x|y_{1:t})\, dx \qquad (3.27)$$

3.2.2. Kalman filter

Kalman Filters (KF) are the most widely used variant of Bayes filters. This type of filter is optimal for linear-Gaussian systems. While a much more fitting case is the Extended Kalman Filter (EKF) which expands the solution for non-linear systems such as the TDoA measurements provided by T4F. Going step by step in the EKF equations, it is possible to start with the definition of both the prior and the posterior pdf as Gaussian:

$$p(u_t|y_{1:t-1}) = \mathcal{N}(\hat{u}_{t|t-1}, P_{t|t-1}) \qquad (3.28)$$

$$p(u_t|y_{1:t}) = \mathcal{N}(\hat{u}_{t|t}, P_{t|t}) \qquad (3.29)$$

In this case the Gaussian pdfs are described by their respective mean value and covariance, thus, the estimation process is accomplished by updating the mean and covariances of the pdfs according to the dynamic and measurement model. If the model is not linear (such

as the case of TDOA measurements), the Extended Kalman Filter is used, thus, the linearized model equations for computing the prediction and update stages are used. In case of TDOA measurement model, the linearization is applied only around the mean value computed in the prediction step $\hat{u}_{t|t-1}$:

$$h_t(u_t) \approx h_t(\hat{u}_{t|t-1}) + \frac{\partial h_t(u)}{\partial u}|_{u=\hat{u}_{t|t-1}}(u_t - \hat{u}_{t|t-1}) \tag{3.30}$$

$$h_t(u_t) \approx h_t(\hat{u}_{t|t-1}) + H_t(\hat{u}_{t|t-1})(u_t - \hat{u}_{t|t-1}) \tag{3.31}$$

The EKF is linearized with a known mean $\hat{u}_{0|0}$ and known covariance $P_{0|0}$. At each interval t, the prediction step and update step are then executed. Once the update step is completed, the position of the target is estimated by using the MMSE estimator (equal to the MAP estimator in this case, being the EKF only applicable to Gaussian distributions) [3]. The prediction step is described by the following equations:

$$\hat{u}_{t|t-1} = A\hat{u}_{t-1} \tag{3.32}$$

$$P_{t|t-1} = A^T P_{t-1|t-1} A + Q \tag{3.33}$$

The update step is then described as follows:

$$G_t = P_{t|t-1} H_t(\hat{u}_{t|t-1})^T (H_t(\hat{u}_{t|t-1}) P_{t|t-1} H(\hat{u}_{t|t-1})^T + R_t)^{-1} \tag{3.34}$$

$$\hat{u}_{t|t} = \hat{u}_{t|t-1} + G_t(y_t - h_t(\hat{u}_{t|t-1})) \tag{3.35}$$

$$P_{t|t} = P_{t|t-1} - G_t H_t(\hat{u}_{t|t-1}) P_{t|t-1} \tag{3.36}$$

The position is then estimated as:

$$\hat{u}_t = u_{MMSE} = \hat{u}_{t|t} \tag{3.37}$$

4 | The T4F project specifics and data analysis

The following chapter describes the details of the main experimental campaign organized for the T4F project. The goal is to test the devices provided by the company in both indoor and outdoor scenarios to verify the related performances for the future applications in more cluttered or industrial environments. The experimental campaign has been carried out to collect real UWB data to assess the performances of Extended Kalman FIlter (EKF) algorithms and compare them with the position provided by the T4F UWB system.

4.1. T4F Localization system

The system in consideration for the localization experiments described in this thesis project is the T4F UWB positioning system. The UWB pack is composed in a set of UWB anchors and tags shown in Figure 4.1. The first represents a set of antennas designed to transmit data packages as well as listening to packets coming from other anchors, based on the time stamps it can compute both information about other anchors position and the very target the system is trying to localize. The tag is an UWB device equipped with an antenna that can use data sent by the anchor's packets of information to calculate and retrieve information about its position. Both the devices are designed to be fast and easy to be used by the final user. The idea is to create a system that is not fixed in one place and can be easily configured according to the user's need. Although the T4F system is originally designed for sport applications, the system can be benchmarked in different scenarios. The goal of the experimental campaign has been to evaluate the the system's performances in a variety of more complex situations, such as more cluttered indoor environments that resembles office-like and industrial scenarios, subject to a series of complexities related to signal loss, fading and harsh propagating conditions.

4.1.1. T4F Anchors

The anchors of the T4F system are a set of UWB antennas which support ranging measurements using both Time of Flight (ToF) measurements based on Two-Way Ranging (TWR), and Time Difference of Arrival (TDOA) measurements. The devices are able to achieve a ranging accuracy of ± 10 cm in Line of Sight (LOS) conditions, supporting up to 6 channel bands from 3.5 GHz to 6 GHz. The devices are composed by the Decawave DWM1000 module, which is based on the Decawave DW 1000 wireless transceiver. The DW 1000 is composed by a single CMOS chip radio transceiver, compliant to the IEEE 802.15.4-2011 UWB standard, which defines the physical and the Media Access Control (MAC) layer for Wireless Personal Area Networks (WPANs) [1]. The system is able to achieve an overall maximum coverage of approximately 60 m by using the channel 4 of frequency range with central frequency of 3993.9 MHz, as shown in Table 4.1, and setting a bit rate of 850 Kb/s.

4.1.2. T4F Tags

A set of tags is also provided for the localization process. Each tag is equipped with the Decawave DWM1001 module, based on the Decawave DW1000 wireless transceiver. The device supports only channel 5 providing a bit rate of 6.8 Mb/s. The module also

Figure 4.1: T4F system: the red boxes indicate tag, anchor and master anchor.

integrates the Nordic microprocessor nRF52832 Bluetooth antenna and the STMicroelectronics LIS2DH12TR three axis linear accelerometer. The location rate depends on the number of active tags, which means that the channel access uses a Time Division Multiple Access (TDMA) scheme, able to change the location rate from 0.01667 to 10 Hz, corresponding to a number of active tags of 9000 and 15 respectively. In conclusion, it is important to report that the maximum coverage of the tag is approximately 60m.

4.2. Geometry and case scenarios

The first campaign is the one related to the indoor experiments. The location chosen was the MADE structure at Politecnico di Milano, campus Bovisa, shown in Figure 4.2. The building is a 2.500 mq indoor space used for co-working, teaching and meetings providing a large number of environments fitting for the desired scenarios because it involves the presence of many obstacles in the way, as well as metal machines and busy areas, perfect for testing a cluttering scenario.The presence of challenging materials and heavy designed environment makes the structure optimal for the experiments.

Two main situations were selected, as illustrated in the map shown in Figure 4.3: an office-like room used for meetings, ideal to test a walking person in a cluttered environment; and one in a more opened space inside the building where the performances were tested on an AGV (Automated Guided Vehicle) which is an industrial machine following a predetermined track.

4.2.1. Indoor acquisitions: office scenario

The first test considers an indoor office, depicted in Figure 4.4, where a table is present in the room's center. The anchors were placed as shown in Figure 4.5, while on the ground a tape was positioned to define a trajectory to be walked by the person equipped with

Channel	Central frequency [MHz]	Bandwidth [MHz]
1	3494.4	499.2
2	3993.9	499.2
3	4492.8	499.2
4	3993.9	1331.2
5	6489.6	499.2
7	6489.6	1081.6

Table 4.1: UWB channels supported by the DWM1000 module.

the UWB tags. The Master anchor is marked in yellow and it is always referred as AP2. For each acquisition, the person to be tracked wore two tags, one placed on the front at the height of the chest and one on the back roughly at the same height, and was moving according to the path highlighted in Figure 4.5. The numbers marked on the yellow

Figure 4.2: MADE building, Politecnico di Milano, campus Bovisa, inside.
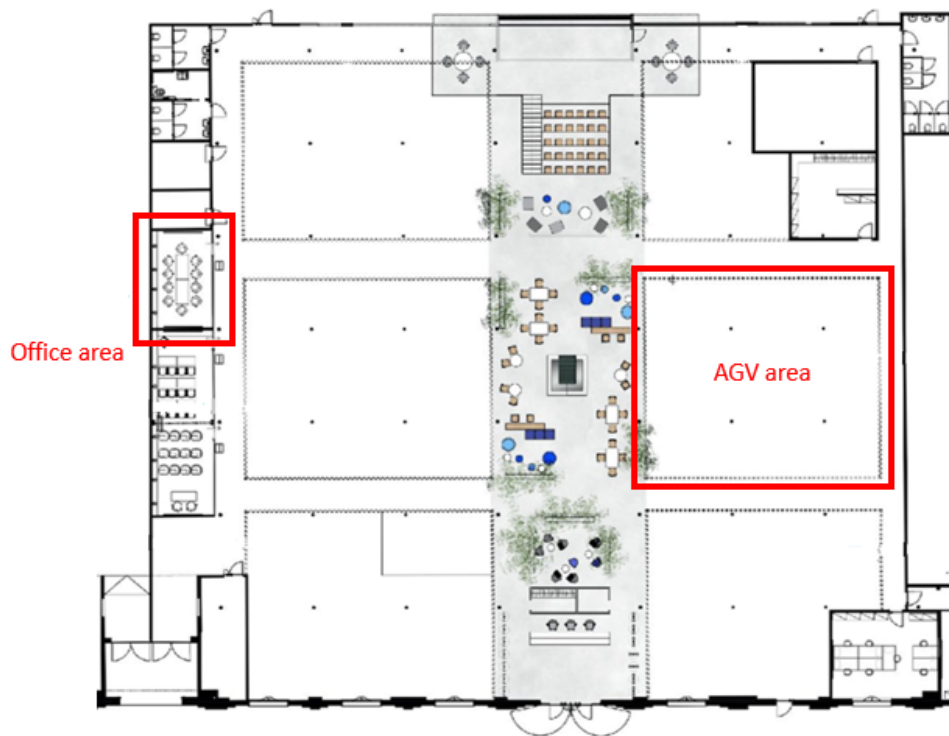
Figure 4.3: MADE building map, Politecnico di Milano, campus Bovisa. Highlighted the areas where the office and AGV experiments were performed.

circles represent the positions of Flying Fish sensors. A Flying Fish sensors is a general purpose proximity sensors, typically used for collision detection. The module consist on an Infra-Red (IR) emitter and IR receiver pair. The output of the Flying Fish is high when the IR signal is detected, thus when the sensor antenna is obscured by an object. The devices were used to keep track of the time-stamps in which the person was passing in the related position. This process was fundamental to synchronize the timing of the T4F data acquisitions, taken from time t_0 every 10ms.

During the test, the user equipped with the tags walks around the table starting from the bottom left corner of the map, following the pre-decided path and completing several loops inside the room.

4.2.2. Indoor acquisitions: AGV

The second acquisition was taken in another part of the MADE structure as shown in the Figure4.6. The area is associated with the one surrounding the pre-calculated path of an AGV (shown in Figure4.7) provided by the facility's staff.

Figure4.8 show the map of the area surrounding the AGV path. The positions of the anchors are similar to the one in the previous experiment, placing the master anchor to

Figure 4.4: Picture of the office room in which the acquisitions were made

the position related to anchor number 2. The AGV machine is able to follow the line (the one in blue in the map) from both sides and to position itself in the middle point of the path. The device moves at a slowly constant velocity and, knowing the actual measures of the followed path it was possible to reconstruct the ground truth positions using the measured data combined to the time information extracted trough a video, as explained in section 4.2.4.
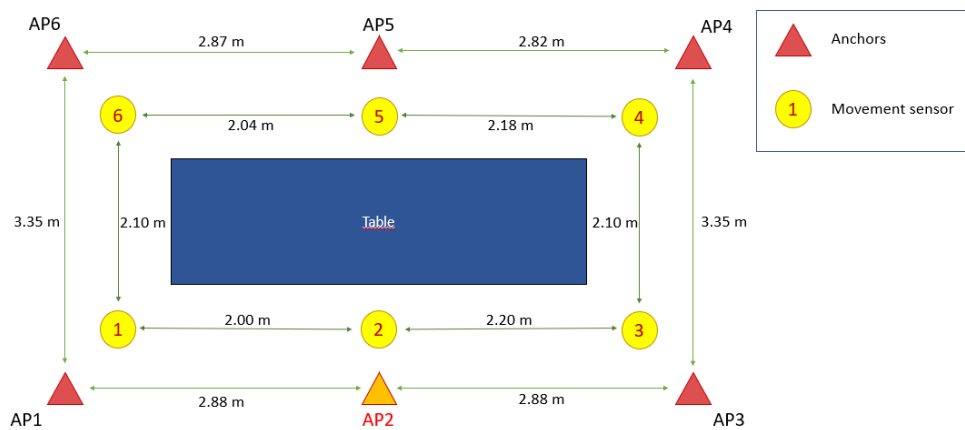
Figure 4.5: Map of the office room where the experiment took place

Figure 4.6: Picture of the area in which the AGV experiments were performed

Figure 4.7: Picture of the AGV used for the experiments

4.2.3. Outdoor acquisitions: volleyball field

The outdoor experiments were made using the volleyball field in the area outside of the very structure of the MADE laboratory in Bovisa campus shown from a top view in Figure4.9. The location was optimal for a sportive scenario testing and including a running target into consideration. The field is shown in Figure4.10 and its map and anchor configuration is reported in Figure4.11. The experiment was made using the same tag configuration as the one proposed in the office acquisition: one placed on the front of
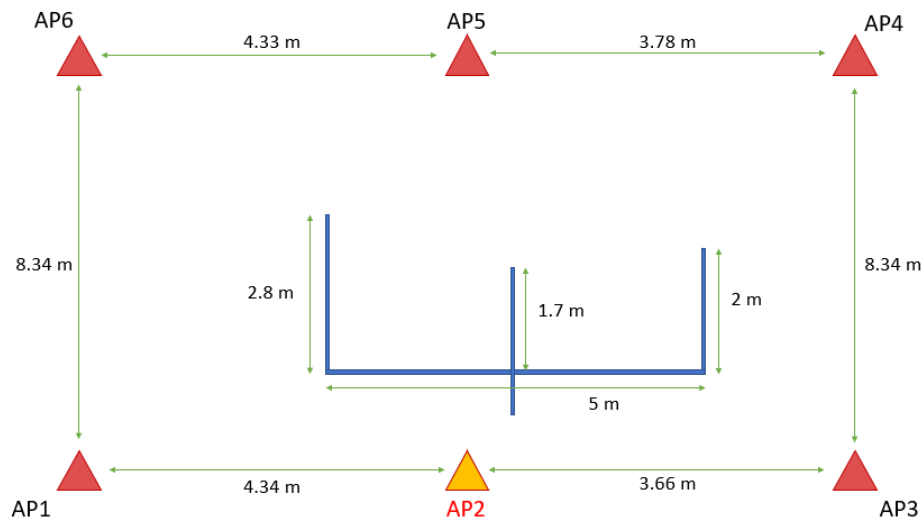
Figure 4.8: Picture of the map of the MADE area in which the AGV was used for the experiments

Figure 4.9: Image extrapolated from the google maps view, showing the area of the outdoor experiments from the top.

the person's chest and on on the back. The target was recorded running trough the field following the white lines shown in Figure4.11. While the experiment was made a video was also taken to extract the ground truth just as for the AGV experiment described in the previous section.

Figure 4.10: Image extrapolated from the video taken during the experimental campaign involving the volleyball field acquisitions
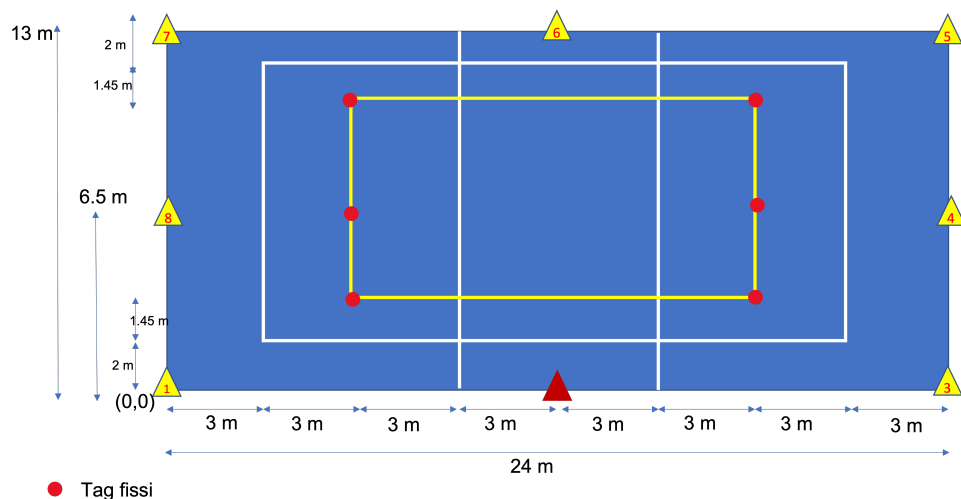
Figure 4.11: Picture of the volleyball field in which the experiments took place.

4.2.4.   Ground truth extrapolation

Extracting the ground truth, meaning the synthetic equivalent of the real path traveled by the related targets to be tracked, was a very important part of the experiments allowing us to use a real path equivalent to unlock the possibility of confront the positions extracted by the tracking algorithms such as the EKF. To do that we used two methods: for the office experiment we used some Flying Fish motion sensors described in Section 4.2.1 placed on the spot marked with a yellow circle in Figure 4.5, while for the AGV and outdoor experiments a video tape was used to extrapolate the time stamps needed to extract the
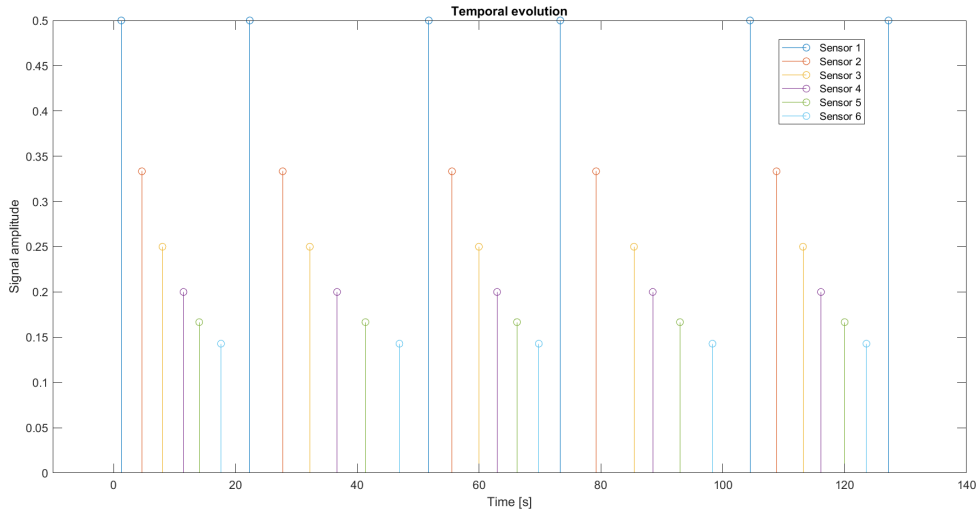
Figure 4.12: Graph representing the time stamps detected by each sensor during the acquisition

positions. Considering the office experiment, the sensor provides a high output to any movement directly in front of its field of view and generates a time-stamp indicating that an object and/or person has been detected, which corresponds to the moment the target is passing in that position. Using MATLAB and elaborating the data, a map of the registered events by each sensor is acquired, showing the temporal evolution of the person walking trough the designated path, as shown in Figure 4.12. The different colors in the figure represents the sensors placed along the path and the amplitudes are different for the sole purpose of better distinguish of each sensor's output.

Subsequently, the time difference between each time stamp is calculated observing the period of time between each registered acquisition. By knowing the traveled distance between each sensor it is possible to extract the corresponding velocity. To extract a faithful ground truth it is also necessary to understand the number of actual useful acquisitions provided by the T4F UWB system. The anchors are able to provide to the user a TDoA signal data, which needs to be elaborated first in order to obtain a reliable position outcome once elaborated trough the use of a tracking algorithm. The data appears in the form shown in Figure 4.13. The structure is a MxN matrix where M is the number of rows representing the corresponding anchors, and M is the number of columns, corresponding to the timestamps of the acquisition, taken each 10ms. The second row is characterized by all NaN (Not a number) elements because it corresponds to the master anchor. It is possible to observe how some of the acquisitions presents different lost data, which also appears as NaN elements in the matrix. The NaN elements may represent actual lost data caused by high noise values or impossibility of elaboration due to sporadic malfunctioning

of the T4F application, or values which resulted too high or too low to be usable (For example if a data appears higher than 10^3 because the time would be too high to be real). The presence of that data if distributed to all the anchor's measurements results on an undefined position.

After that, it is also necessary to define, observing the data, the number of actually available acquisitions between each marked point shown in Figure 4.5. Therefore, to calculate the exact number of acquisitions available between each segment of interest it was necessary to run the EKF algorithm at least once to generally track the overall position evolution and physically count the number of available positions present between each marked point. This allowed us to connect each predicted position to their relative acquisition time-stamp. The goal of this process was to estimate the actual number of positions we needed to have in the synthetic path in order to reconstruct a believable ground-truth and have a one-to-one correspondence with the available data.

For what concerns the AGV, we used a video recording of the acquisition, as shown in Figure4.14. The video was taken at the same time of the start of the T4F system. Studying the positions and the measurements taken on the map of the related area of interests it was possible to extract a series of time stamps using the video's timeline. Once again, comparing with the available measurements of the TDoA data, it was possible to reconstruct a one-to-one correspondence between the estimated positions and the synthetic ground-truth coordinates.

The outdoor acquisition was also made using a similar method as the AGV one. The video provided the time stamps to take into consideration into the construction of the synthetic path.

4.3. Data analysis and filter calibration

The data provided by the system are affected by noise. The tag response to the main anchors is also something to take into consideration, given the fact that not all the devices

	1	2	3	4	5	6	7	8	9	10
1	NaN	-2.4444	NaN	-2.4191	-2.6327	-2.5524	-2.4643	-2.1676	-2.2634	-2.1653
2	NaN	NaN	NaN	NaN	NaN	NaN	NaN	NaN	NaN	NaN
3	NaN	2.0722	1.7669	2.2981	1.8944	2.5453	2.3947	2.6739	2.0601	2.3383
4	NaN	3.5972	3.5207	3.5898	2.6061	2.7166	2.7049	3.0140	2.9303	3.0220
5	NaN	1.0246	0.4360	1.1351	0.9228	1.0224	1.0227	0.5223	1.3164	1.4551
6	NaN	-0.5498	-0.5108	-0.5100	-0.6731	-0.6032	-0.4633	-0.1496	-0.2284	-0.0726

Figure 4.13: Extract from the set of data provided by the T4F system in MATLAB, showing the TDoA values

are able to give reliable data. Part of the testing was in fact connected to the elimination of the unusable data derived directly from the measurements. The unreliability of the tags might depend on the internal malfunctioning of the devices, the disturbances caused by the surroundings (such as the presence of obstacles or the multi-path fading phenomenon) or even some issues with the elaboration of the data trough the application.

4.3.1. Missing data managing

When the information is available it is important to eliminate the missing data from each AP. The removal of the NaN elements and the outliers, such as data in which the time of arrival is incredibly high ($\geq 10^3$), or incredibly low ($\leq 10^{-3}$). It is possible to use the TDoA data up to the point in which only two measurements are available, otherwise the whole measurement must be discarded.

4.3.2. Covariance estimation

Diving into the more technical detail, the filtering algorithm is the main developed feature. The EKF needs to be calibrated, therefore it is necessary to introduce as input the right driving process variance to match the movement of the target with respect to the actual model used, and the covariance matrix to describe the noise impacting the measurements.

The latter is calculated using as a tool the measurements made performing a static tag acquisition. During the campaign some data were gathered keeping the tags in a fixed

Figure 4.14: Image extrapolated from the video taken during the experimental campaign involving the AGV acquisitions

place, allowing us to know the actual position of the devices calculating the error difference of the TDoA measurements. Calculating the distance from each anchor to the ground truth position (as TOA) and subtracting the one associated to the master anchor, we obtain the true TDoA data, from which we can compare to the actual measured data appearing as shown in Figure 4.13. From this result it is possible to calculate the mean and the variance of the error, building a covariance matrix usable for all the acquisitions related to the indoor experiments. The covariance matrix is built starting from the calculation of the error between the two TDoA measurements by simply computing the difference between the two set of data. Then the mean is calculated as:

$$x_{mean} = \frac{1}{N} \sum_{k=1}^{N} \epsilon_k \tag{4.1}$$

where N is the number of available acquisitions (excluding the one with the discarded data) and ϵ_k is a matrix containing all the errors of the measurements. The covariance matrix R is obtained trough:

$$R = \frac{1}{N-1}(\epsilon - \epsilon_{mean})(\epsilon - \epsilon_{mean})^T \tag{4.2}$$

where ϵ_{mean} is the mean error calculated. The covariance matrix from the experimental data has the following values:

$$R = \begin{bmatrix} 0.8816 & 0.5342 & 0.3887 & 0.7599 & 0.5732 \\ 0.5342 & 1.6063 & 0.7085 & 1.2948 & 0.3436 \\ 0.3887 & 0.7085 & 1.2257 & 0.7299 & 0.5471 \\ 0.7599 & 1.2948 & 0.7299 & 1.9343 & 0.8060 \\ 0.5732 & 0.3436 & 0.5471 & 0.8060 & 1.2989 \end{bmatrix} \tag{4.3}$$

For what concern the outdoor scenario, a similar experiment was made. To extrapolate the measurement error in that case, some static tags were placed throughout the area in consideration. The aim was still to calculate the positioning error knowing the exact position of the tags on the map comparing the actual TDoA measurements and calculating the relative error. In this case we obtain a 7x7 matrix because we used eight anchors instead of the six used for the indoor acquisitions. The dimension count one less row and column with respect to the number of anchors because with the TDoA measurement one of the anchor is seen as the reference one and does not appear into the full matrix used in the algorithms.

$$R = \begin{bmatrix} 0.1999 & 0.2420 & 0.3296 & 0.1387 & 0.0547 & 0.0482 & 0.1043 \\ 0.2419 & 0.3266 & 0.2896 & 0.1830 & 0.0705 & 0.0571 & 0.1349 \\ 0.2195 & 0.2896 & 0.2695 & 0.1674 & 0.0678 & 0.0544 & 0.1231 \\ 0.1387 & 0.1830 & 0.1674 & 0.1087 & 0.0467 & 0.0365 & 0.0779 \\ 0.0547 & 0.0705 & 0.0678 & 0.0467 & 0.0367 & 0.0268 & 0.0354 \\ 0.0481 & 0.0571 & 0.0544 & 0.0365 & 0.0268 & 0.0325 & 0.0368 \\ 0.1043 & 0.1349 & 0.1231 & 0.0779 & 0.0354 & 0.0368 & 0.0725 \end{bmatrix} \tag{4.4}$$

We observe that for the indoor acquisitions a mean error on the measurements of 0.14 m is obtained, while for the outdoor we get a mean of 0.15 m. The overall error estimate appears to be the same, but the outdoor acquisitions required the elimination of some important outliers increasing the mean error of some more meters for the outdoor results. As discussed later on in Section 5.4, the main problem of the outdoor acquisition is not related solely to the measurement but especially to the loss of a big part of the information concerning a big amount of missing measurements.

4.3.3.   Driving process variance estimation

The next step is estimate the driving process variance. For this purpose it is necessary to use the ground truth to calculate the position error from the actual acquisition and iterating the process for different values of such variance. The following table show the selected values chosen for different driving process for which the CDF presented a better positioning error value. The CDF was calculated using the empirical cumulative distribution function, defined as:

$$\hat{F}_n(t) = \frac{n_s < t}{n} = \frac{1}{n} \sum_{i=1}^{n} 1_{x_i <= t} \tag{4.5}$$

Where n_s is the number of element per sample, $1_{x_i <= t}$ is a Bernoulli random variable expressing the case in which the random variable X_i is less or equal than t. Therefore $n\hat{F}_n(t)$ is a binomial random variable with mean nF(t) and variance nF(t)(1-F(t))., which means that $\hat{F}_n(t)$ is an unbiased estimator of the error. We can then define the mean of the empirical distribution as an unbiased estimator as:

$$E_n(X) = \frac{1}{n} \sum_{i=1}^{n} x_i \tag{4.6}$$

and the variance as:

$$Var(X) = E[(X - \hat{x})^2] = \frac{1}{n}(\sum_{i=1}^{n} x_i - \hat{x})^2 \tag{4.7}$$

From this calculation we can select the best error performances from deriving from the EKF algorithms calculating the position error directly from the final data and select the results with the best error solution. As a consequence of that we obtain the following values for the driving process to be selected for the EKF, reported in Table4.2

Scenarios	Random velocity process variance	Random acceleration process variance	Random turn process variance
Uffici	$0.83 \ m/s$	$1m/s^2$	$1 \ m/s^2$
AGV	$1 \ m/$	$1 \ m/s^2$	$1 \ m/s^2$

Table 4.2: Table of the driving process standard deviations for all the used models in the experimented scenarios.

5 | T4F project experimental results

In this chapter the main results of the experimentation campaign are shown. The goal is to test the EKF algorithm and compare with different methods (such as a LS algorithm and the data elaborated by the T4F application) to prove the filtering is in fact improving the localization performances. The data for each method are elaborated and an error CDF (cumulative density function) is calculated comparing the positions with the ground truth previously generated and the respective RMSE and CEP95 values. The objective resides into the demonstration that the filtering algorithm is actually improving the performances of the UWB system, compare different motion models and study the difference between the results in position calculated by us, considering the real anchor's positions, and the one resulting from the T4F system's auto-localization of the anchors.

Both the indoor and outdoor results are shown, starting from the Office acquisitions in Section 5.2, to the ones related to the AGV in Section 5.3 and finally the outdoor results concerning the volleyball field in Section5.4.

5.1. Experimental results

The results are shown in the following way: First an overview on the response of the algorithm to different motion models is proposed. This is important because it is needed to find out which motion model is actually performing the best. To do that we use the help of graphical representation of the different position paths generated by the model's application to the EKF algorithm and the estimation of the error CEP95 (Circular error probable) to actually get a numerical evaluation of the position error. Secondly, the actual performance of the tags are evaluated comparing the EKF result obtained with the use of an optimal motion model, to different localization methods, such as an LS algorithm and the results provided by the T4F system itself elaborated trough it's application.

Before proceeding, it is important to briefly describe the Least square algorithm used to

perform the localization for the purpose of confrontation. The technique has the goal to minimize the sum of the square residuals, with the aim to measure the level of variance in the error term, or residual, of a regression model. The type of algorithm used is the Gauss-newton **??**, providing a non-probabilistic technique for position estimation, following the steps:

- Linearize the measurement model from the TDoA data as:

$$\mathbf{y} \approx \mathbf{h}(\mathbf{u}_{n-1}) + \mathbf{H}(\mathbf{u}_{n-1})(\mathbf{u} - \mathbf{u}_{n-1}) + \mathbf{n} \tag{5.1}$$

  which becomes:

$$\Delta y = y - h(\mathbf{u}_{n-1}) = \mathbf{H}(\mathbf{u}_{n-1})\Delta u + \mathbf{n} \tag{5.2}$$

  where $\mathbf{H}(\mathbf{u}_{n-1})$ is:

$$\mathbf{H}(\mathbf{u}_{n-1}) = \begin{bmatrix} \frac{\partial h_1(\mathbf{u}_{n-1})}{\partial u_{n-1}} \\ ... \\ \frac{\partial h_{M-1}(\mathbf{u}_{n-1})}{\partial u_{n-1}} \end{bmatrix} \tag{5.3}$$

  being h(u) the measurement model (TDoA in this case) and M the number of anchors. While $\Delta u = \mathbf{u} - \mathbf{u}_{n-1}$.

- Minimizing the Least Square over the new model we can obtain:

$$\mathbf{u}_n = \underset{\mathbf{u}}{\mathrm{argmin}} ||\Delta y - \mathbf{H}(\mathbf{u}_{n-1})\Delta u||^2 \tag{5.4}$$

- The update is then recursively performed using the equation:

$$\mathbf{u}_n = \mathbf{u}_{n-1} + (\mathbf{H}(\mathbf{u}_{n-1})^T\mathbf{H}(\mathbf{u}_{n-1}))^{-1}\mathbf{H}(\mathbf{u}_{n-1})^T\Delta y \tag{5.5}$$

  After performing a number of iteration starting from a random initial solution, the process stops when a certain error $||\mathbf{u}_n - \mathbf{u}_{n-1}||$ threshold is reached.

In addition for this, other representations are illustrated to help visualizing the actual evolution of the path and the tracking effect of the filter over the other methods and visualize the positioning error for at each time instant. To this purpose a visualization with connected points and a visualization of the prediction covariance trough the plotting of the relative error ellipse for each position are proposed.

Lastly the comparison of the performance in terms of position error and visual representation is also performed with respect to the differences obtained from the localization using the real anchor's positions and the one estimated trough the auto-localization algorithm

provided by T4F.

All of the above are repeated for each available acquisition and each available tag for both the indoor and outdoor experiments.

5.2. Office acquisition analysis

As reported in Figure4.5 the layout of the office allowed us to take different acquisitions regarding a path around the office itself. The target is completing four loops around the table placed at the centre of the room. The experiments is repeated for two tags placed in the front and the back of the subject.

5.2.1. Office: motion models comparison

Before showing the results a preparatory analysis had to be done: testing the different motion models to determine the best one to use in the final evaluation. The picked models are the ones described in section 3.1:

The motion model's equations were placed into the EKF algorithm, explained in Section 3.2.2, and used predict the position of the target in each time instant. The difference in path between the models for both tag 1 and 2 of the office experiments are shown in Figure5.1 for tag 1 and Figure5.2 for tag 2. The positions estimated for the three models are plotted, highlighting the differences between the three different predicted paths. We can easily observe how the random walk model is performing better than the other two
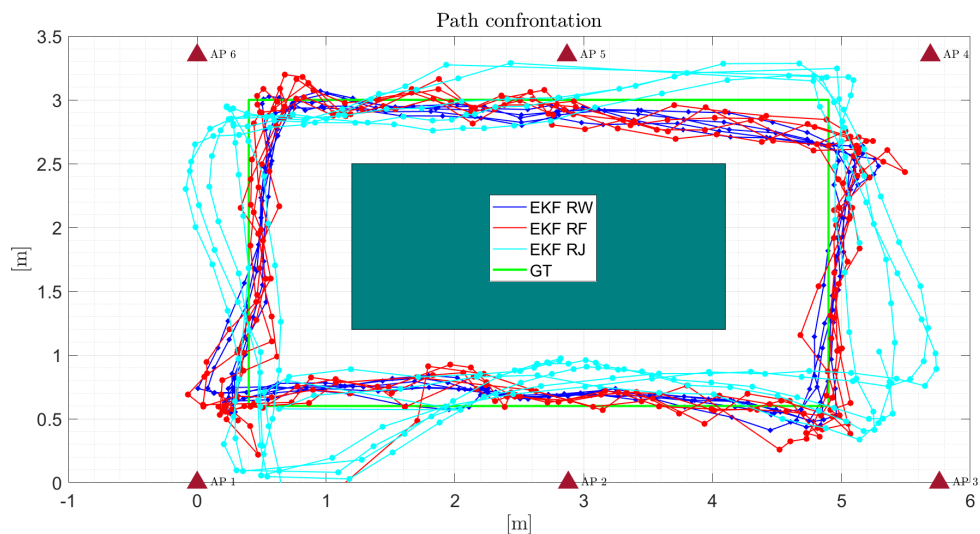
Figure 5.1: Plot of the different motion models path used for the tag 1 of the office acquisitions.

models. This is because the random walk is the most suited one to describe a walking target. The walk gait is not uniform, therefore it is not good to assume a constant velocity into the model. To ensure that the KF works properly it needs to take as an input a model that resembles the target's one so that the prediction step of the filter can be optimized. Unless the use of a different inertial sensor is included (such as a velocimeter, accelerometer or a gyroscope) in order to adapt the new information into the algorithm, the filter will perform worse. Observing the two figures we can see how the random force model does not give a good enough performance in the curves since the target is changing direction, and therefore velocity, faster than it's normal gait in the straight path. The Jerk model instead considers a constant acceleration of the target which results in a much more accentuated deviation of the path.

The related CDFs were also plotted, calculated as explained in Section 4.3.3, comparing the positions with the ground truth, we can see how the performance of the three models returns higher errors for the random force and random jerk models.

The error is calculated doing the difference between the position coordinates of the related data and the ground truth one, while the position error is calculated as:

$$\epsilon_p = ||\hat{\mathbf{u}} - \mathbf{u}|| \tag{5.6}$$

where $\hat{\mathbf{u}}$ is the estimated position (from the EKF) and $\mathbf{u}$ is the real position (Ground truth) The CDFs were used to calculate the CEP 95. This parameter, defined as the circular
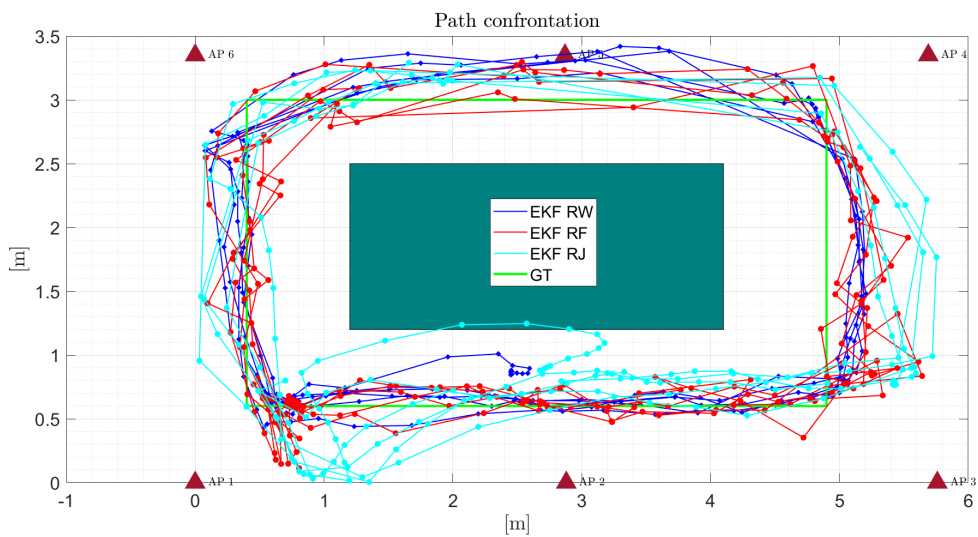
Figure 5.2: Plot of the different motion models path used for the tag 2 of the office acquisitions.

error probable, provides the measure of the accuracy of a position in a localization system. It gives in response the measure of the radius of a circle containing the position estimate with a probability of 95%. The CEP95 is the radius of the circle corresponding to the confidence level P, defined as:

$$P[|\Delta\mathbf{u}| <= CEP_p] = P \tag{5.7}$$

Where P is the percentage probability of fixes within a circle of radius CEP_p around the true location. The CEP95 can be approximated as:

$$CEP_{95} \approx 2\sigma_H \tag{5.8}$$

Where σ_H is the horizontal root mean square error (HRMS) defined as:

$$\sigma_H = \sqrt{\sigma_x^2 + \sigma_y^2} = \sqrt{\lambda_1^2 + \lambda_2^2} \tag{5.9}$$

where σ_x, σ_y are the error with respect to the x and y coordinate and λ_1, λ_2 are the length of the semi axes of the error ellipse representing having as eigenvalues $\lambda_i^2 = eig_i[C]$ with C the covariance matrix of the prediction error. In this case the CEP95 for each method can be also easily calculated graphically trough the cumulative density function, looking at the intersection with of the functions with the value of probability of 0.95, as shown in Figure 5.3 for tag 1 and in Figure 5.4 for tag 2.
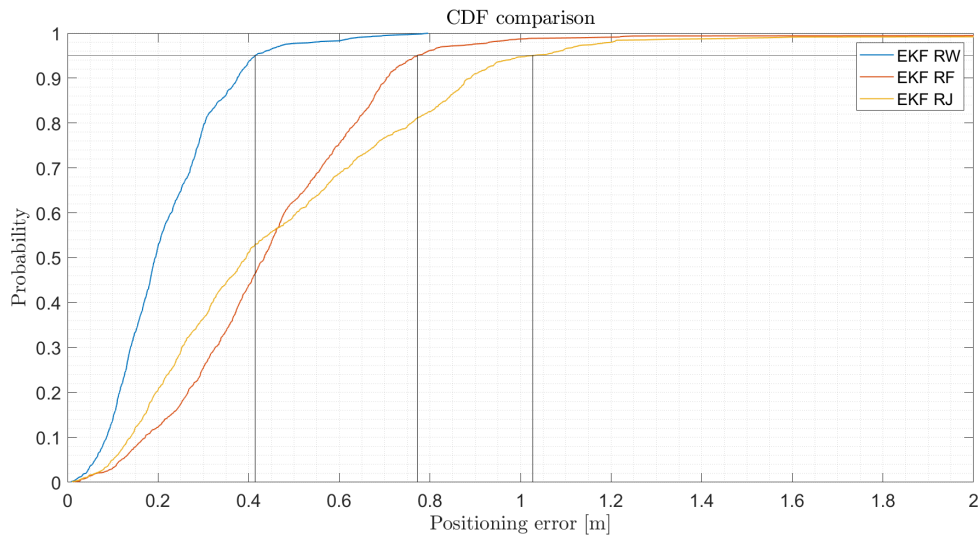
Figure 5.3: Cumulative density function of the position error respectively for the EKF Random walk, EKF random force and EKF random jerk model positions compared to the ground truth.
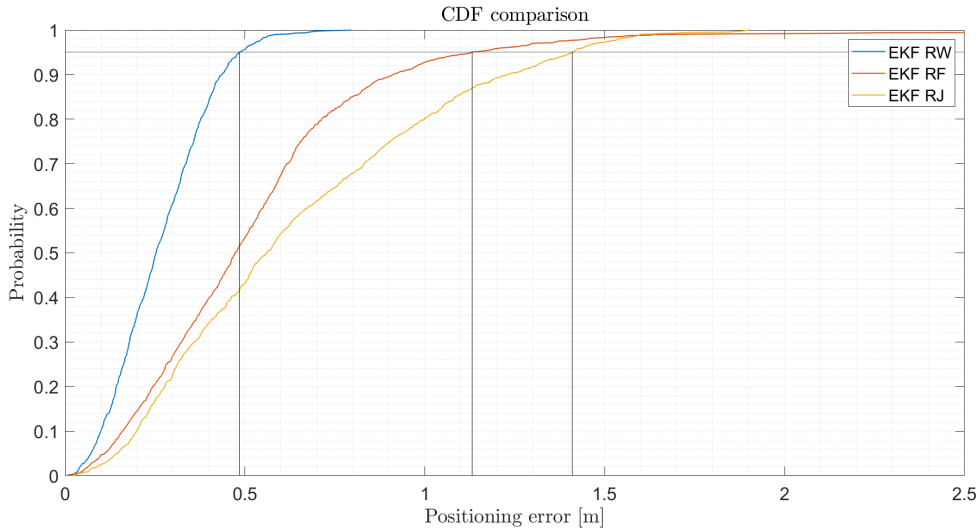
Figure 5.4: Cumulative density function of the position error respectively for the EKF Random walk, EKF random force and EKF random jerk model positions compared to the ground truth.

For the tag 1 the CEP95 values are the following:

- EKF RW: CEP95 = 0.41m

- EKF RF: CEP95 = 0.77m

- EKF RJ: CEP95 = 1.03m

For the second tag we obtain:

- EKF RW: CEP95 = 0.48m

- EKF RF: CEP95 = 1.13m

- EKF RJ: CEP95 = 1.14m

From these values it is evident that the Random walk model is in fact the best solution to pick. The model fit the motion characteristic of the target and is providing the smaller position error values, therefore it is chosen to be tested for all the other experimental results and confrontations shown in the following paragraphs.

5.2.2.   Office: general results

The following pictures show the position of the tag throughout the experiment. Three different techniques are highlighted:

1. Positions related to the EKF using a random walk model in blue.

2. Positions related to the LS algorithm in red.

3. Positions related to the T4F raw data extrapolated from the application in cyan.

Figures 5.5, 5.6 and 5.7 show how the trajectories are following the ground truth path. The EKF algorithm presents a better tracking path, characterized by a smoother line and highlighting the prediction process implemented by the adaptive filter.

The next step has the objective of providing a quantification of the position error cal-
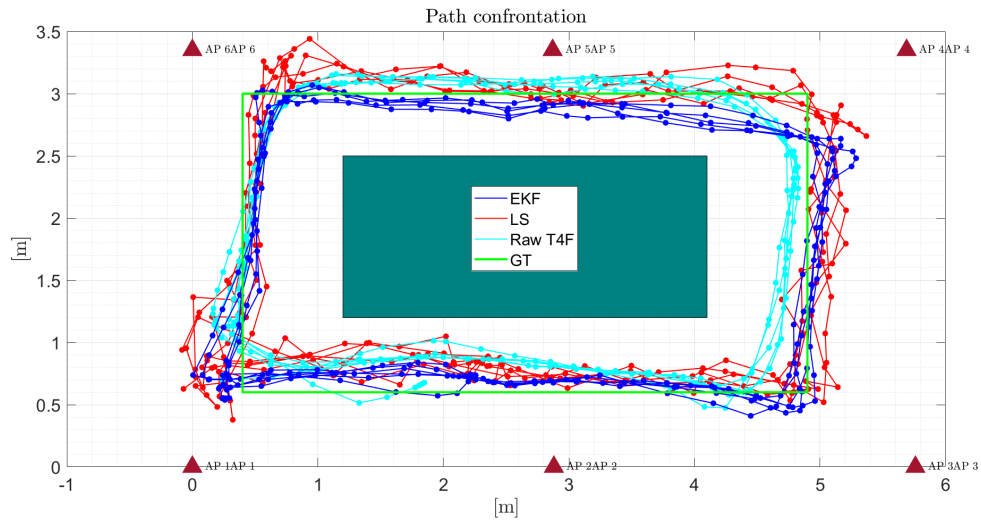
Figure 5.5: Path difference of the office acquisition for tag 1. Highlighted EKF with a random walk model, LS algorithm, T4F raw data results and estimated ground truth path.
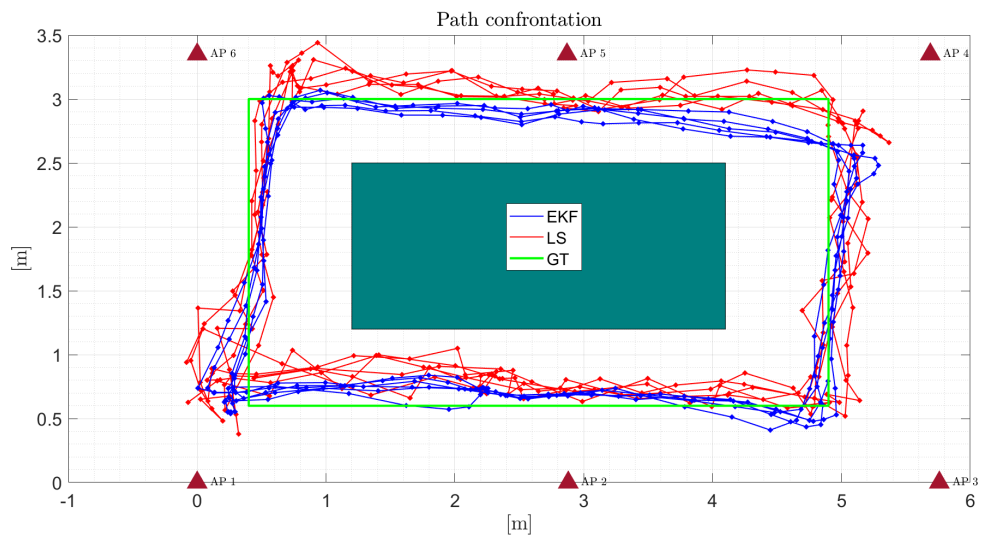
Figure 5.6: Path difference of the office acquisition for tag 1. Highlighted EKF with a random walk model, LS algorithm and estimated ground truth path.

culated for the campaign. The following picture shows the CDF of the position error calculated respectively for the EKF, in the case of a random walk model used, for the LS algorithm results and the Raw T4F data. The CDF appears as shown in Figure5.8:

In this case the CEP95 for each method can be easily calculated trough the cumulative density function and corresponds to:

- EKF: CEP95 = 0.41m

- LS: CEP95 = 1.02m
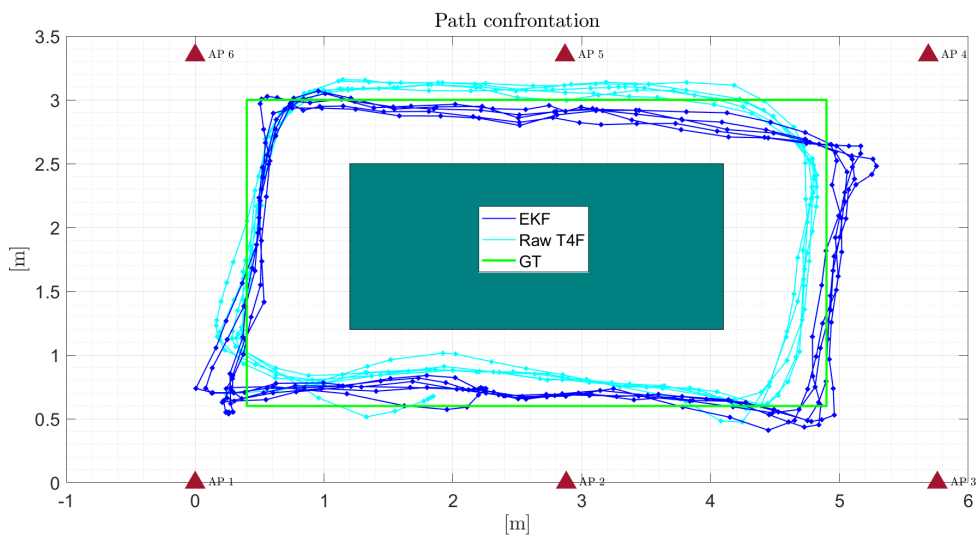
Figure 5.7: Path difference of the office acquisition for tag 1. Highlighted EKF with a random walk model, T4F raw data results and estimated ground truth path.
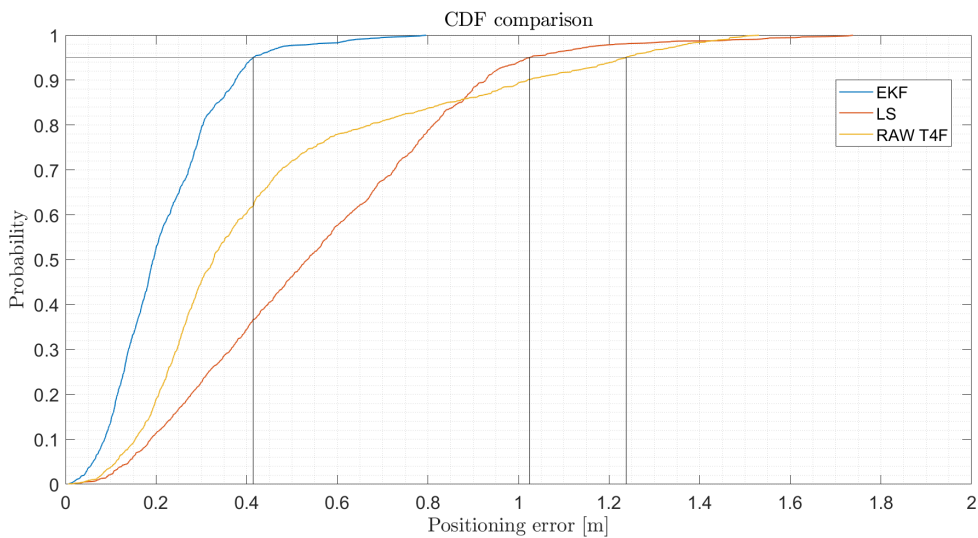
Figure 5.8: Cumulative density function of the position error respectively for the EKF, LS algorithm and T4F raw data compared to the ground truth.

- Raw T4F: CEP95 $= 1.23$m

It is possible to observe that the Kalman filter improves the accuracy of the localization, performing under the 1 meter boundary and outperforming both the LS algorithm and the T4F system's positions.

One more representation that it is possible to implement to observe the improvement of the tracking procedure of the adaptive filtering is the following: Connecting the points in a one-to-one correspondence with the ground truth can highlight the difference between the performance of the LS algorithm (Figure5.10), which will provide a noisier, and the EKF (Figure5.9), providing a smoother tracking.

Lastly, using the representation of the trace of the prediction covariance, it is possible to draw the error ellipse related to the current position predicted by the selected Kalman filter or eventually by the LS algorithm. This visualization is important because it returns a graphical representation of the evolution of the positioning error during the tracking process. Trough the ellipse's shapes we can appreciate how much the error is impacting on the positioning with respect to both coordinates x and y. Each error ellipse can be defined by the following parameters: center position, heading and magnitude of the semi-axes. The ellipse can give a good graphical representation of the precision of a position fix, where the amount of flattering of the latter along one dimension can indicate the increased error related to the associated coordinate of the position [6]. The parameters of the error ellipse are determined trough the eigenvalue and eigenvector evaluation. We can say that the roots of eigenvalues of the covariance matrix of the position corresponds
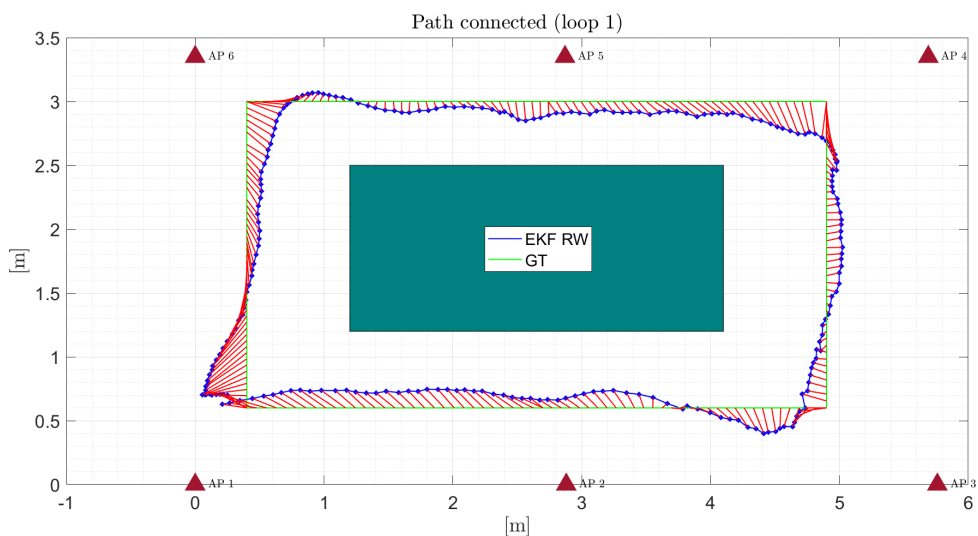
Figure 5.9: Plot of the connected path between the EKF positions and the ground truth for the first loop of the related target.

to the lengths of the error ellipse axes, while the eigenvectors define the direction of the error ellipse axes. Considering the covariance matrix:

$$C = \begin{bmatrix} \sigma_{xx}^2 & \sigma_{xy}^2 \\ \sigma_{yx}^2 & \sigma_{yy}^2 \end{bmatrix} \tag{5.10}$$

where C is the covariance matrix, σ_{xx}^2 and σ_{yy}^2 are respectively the error variance along the x and y axes, while σ_{xy}^2 and σ_{yx}^2 are the cross error variances between the two dimensions. The error ellipse equation can be written as:

$$(\frac{x}{\sigma_{xx}^2})^2 + (\frac{y}{\sigma_{yy}^2})^2 = s \tag{5.11}$$

where s is a scaling factor of the ellipse and the rotation angle of the ellipse is calculated as:

$$\theta = \frac{1}{2} arctan(\frac{2\sigma_{xy}^2}{\sigma_{xx}^2 - \sigma_{yy}^2}) \tag{5.12}$$

The following representation, shown in Figure5.11 provides a visualization of the error ellipses for the first loop of the office acquisition for the first tag, highlighting the results for just the first loop computed by the target. This representation gives a good idea of how small the error is for each position predicted by the Kalman filter. The error only increases in the proximity of some of the curves, which are in fact the most critical placements of the map for the localization.
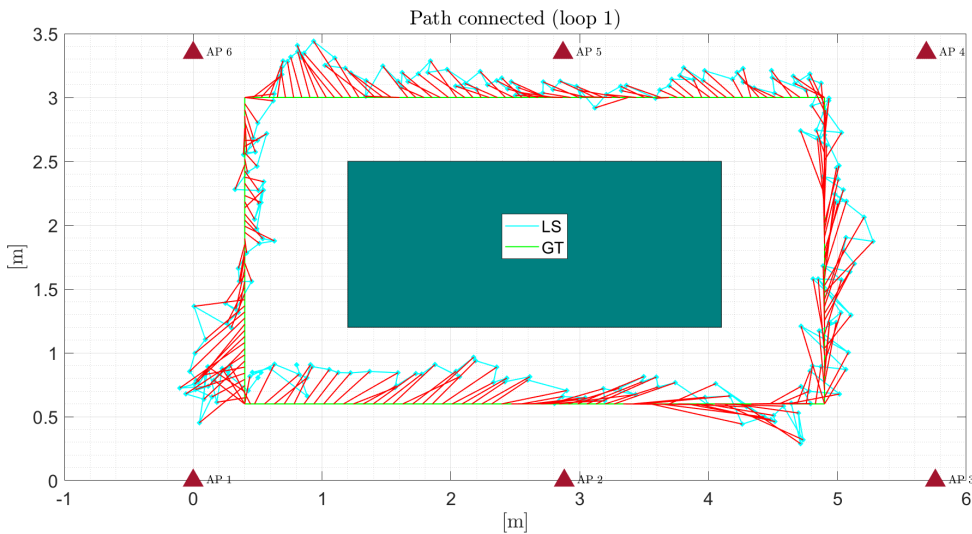
Figure 5.10: Plot of the connected path between the LS positions and the ground truth for the first loop of the related target.

For what concerns the second tag, the following graphs represents the obtained results of the positioning confrontation. As for the first tag, Figure 5.12 represents all the methodology (EKF, LS and T4F positions) superposed, while Figure 5.13 and Figure 5.14 are showing the comparison with the singular methodologies.

For this tag also the results for the path confrontation provide a visual understanding of
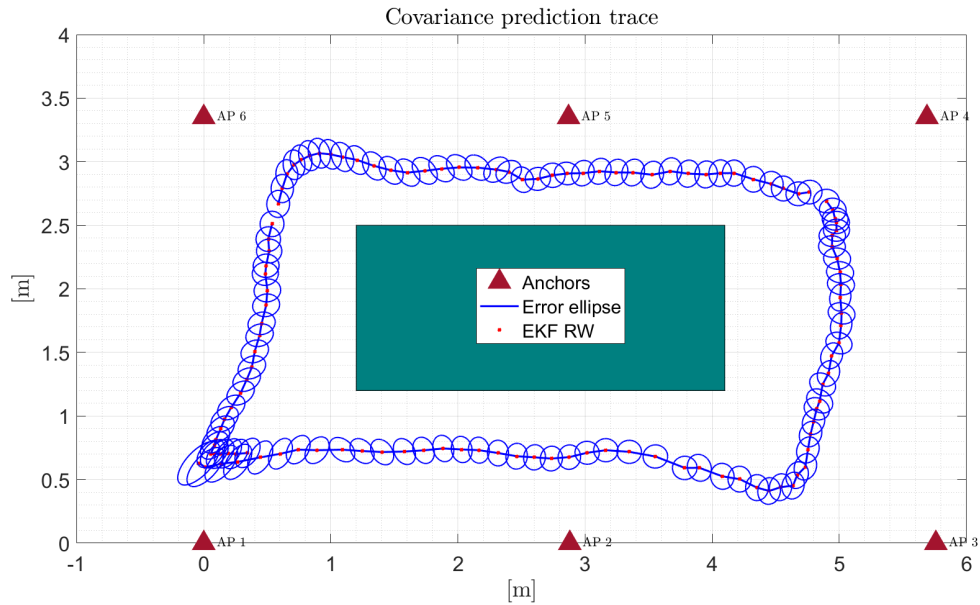
Figure 5.11: Plot of the trace of the prediction covariance for each estimated position of the EKF using the random walk model for the office acquisition, tag 1, first loop.
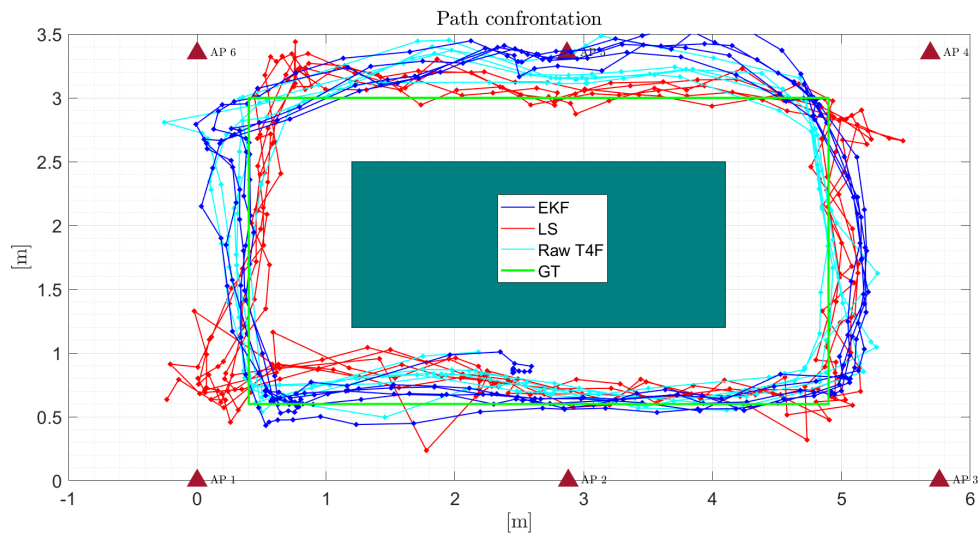
Figure 5.12: Path difference of the office acquisition for tag 2. Highlighted EKF with a random walk model, LS algorithm, T4F raw data results and estimated ground truth path.

how the filtered results gives a better tracking. It is evident that the second tag does not have as good performance as the previous one and this is also proven by looking at the correspondent CDF result in Figure5.15:

The CDF results presents a slightly worst results with respect to the other tag, especially for the T4F data positions which increase the error over the 2 meters threshold. The CEP95 values calculated are the following:
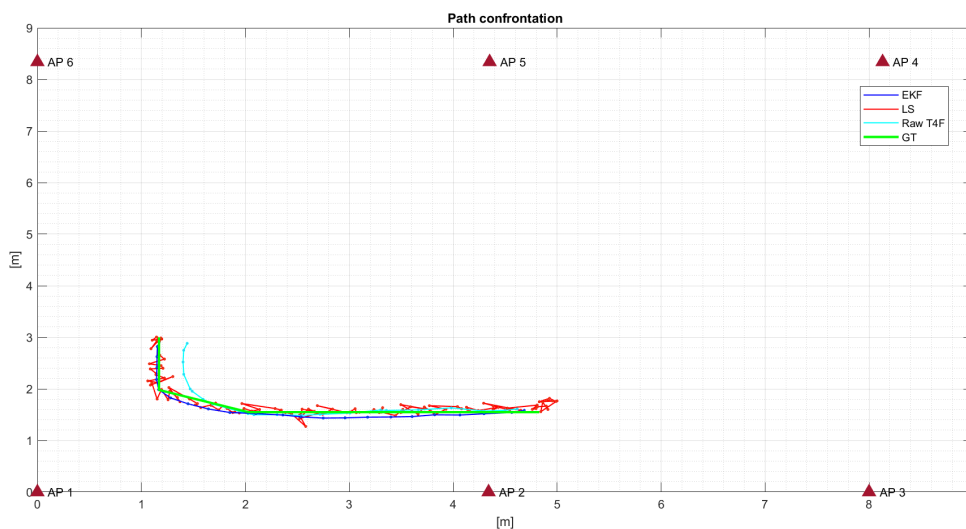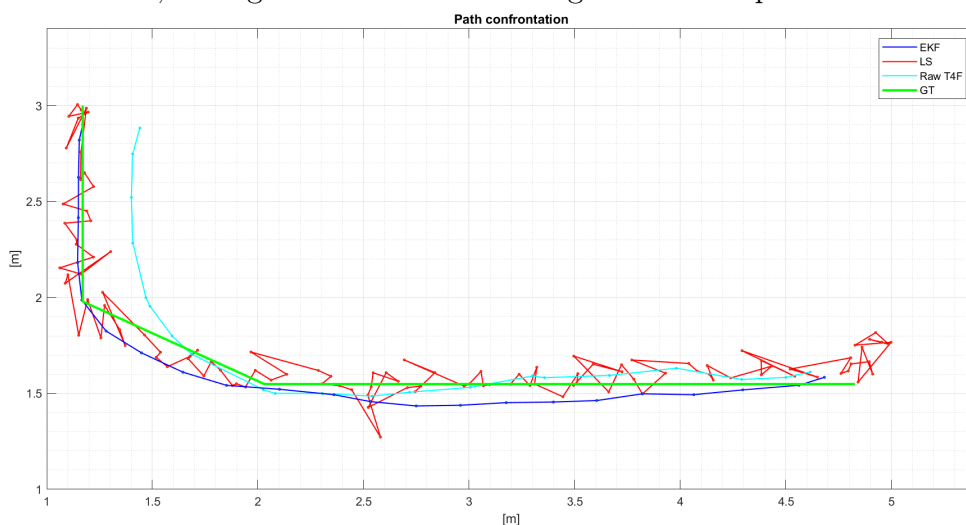
- EKF: CEP95 = 0.48m
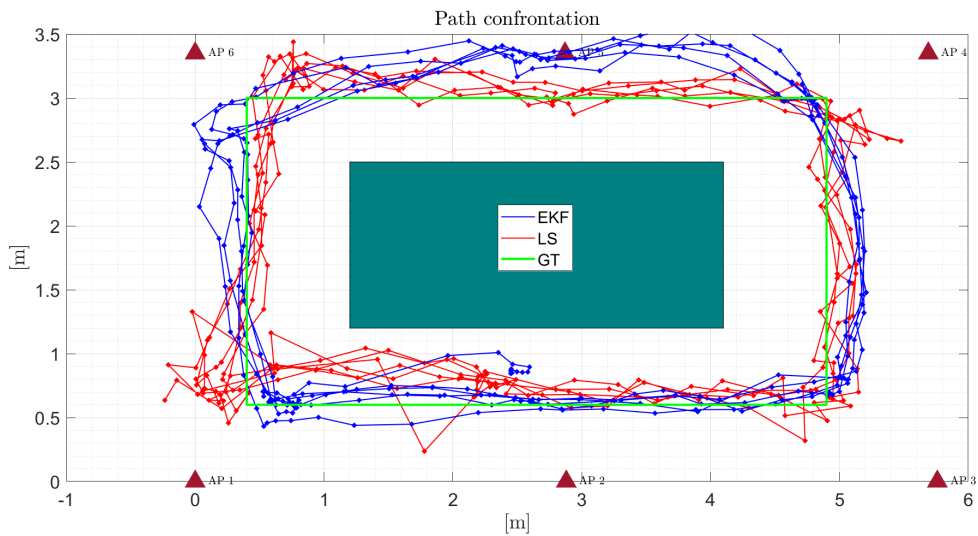
Figure 5.13: Path difference of the office acquisition for tag 2. Highlighted EKF with a random walk model, LS algorithm and estimated ground truth path.
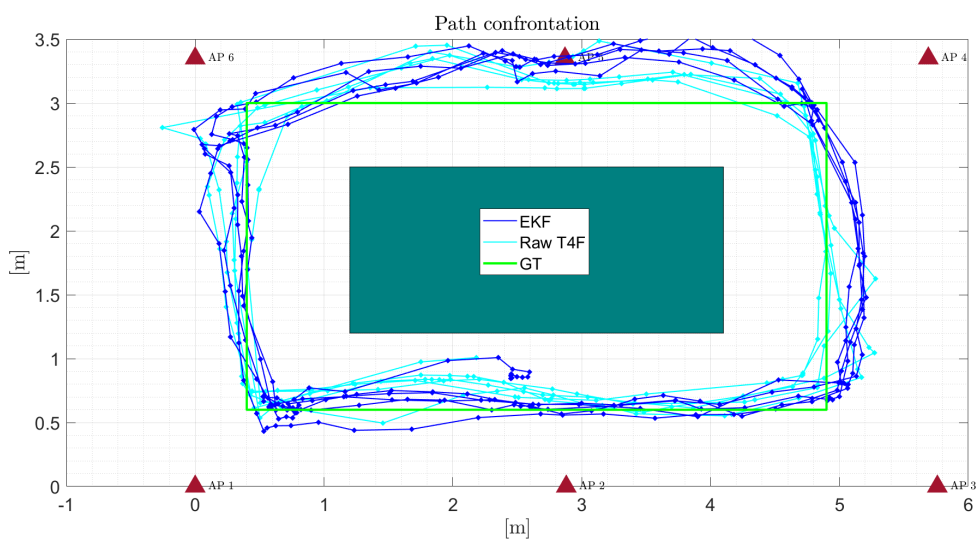
Figure 5.14: Path difference of the office acquisition for tag 2. Highlighted EKF with a random walk model, T4F raw data results and estimated ground truth path.

- LS: CEP95 = 1.02m

- Raw T4F: CEP95 = 2.03m

Also in this case the EKF localization result appears to perform better than the rest. According to the results, the T4F trajectory provides unsatisfactory performances in the considered scenario and cannot be utilized for high-accuracy location services.

For what concerns the connected path representation, we obtain the visualization shown in Figure5.16 and Figure5.16 which reports respectively the one-to-one connection between the EKF positions to the ground truth and the LS positions to the same synthetic path. Both visualizations are referred to the first loop and the disordered nature of the LS solution is easily highlighted in the plots.

Following, we have the trace of prediction covariance representation in Figure5.18, featuring the error ellipses calculated for each position for the first loop of the acquisition.

Since the second tag of the office experiment, as demonstrated from the previous results, is in fact less performing, the error ellipses for each position results more stretched and distorted due to the increased error along one of the axis.

5.2.3. Office: anchors position confrontation

The T4F system also provides an auto-localization algorithm previously developed. The auto-localization phase's purpose is to automatically find the anchors positions using a set
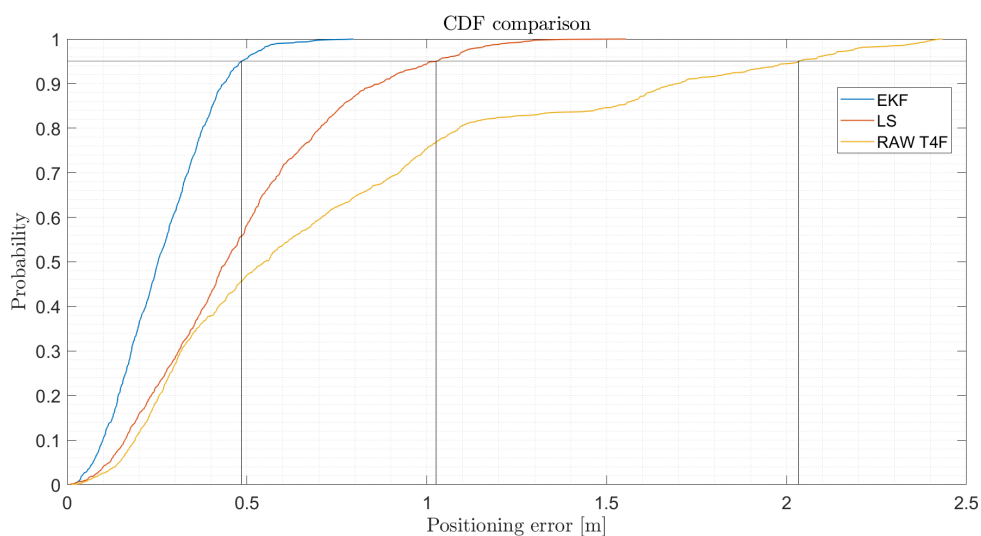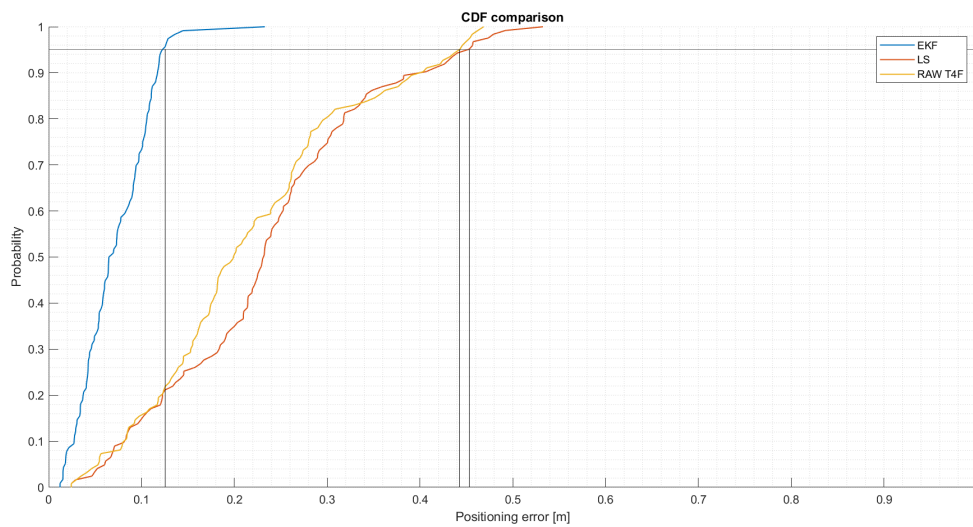

Figure 5.15: Cumulative density function of the position error respectively for the EKF, LS algorithm and T4F raw data compared to the ground truth.

of corrected ranging measured. The process consists on an isolation forest algorithm for the outlier detection and filtering and a anchor positioning method based on the following steps[9]:

- Take two reference anchors, the number of anchors M and the matrix $\hat{D}$ containing all the sample mean between each anchor pair as input.

- compute a minimization problem solution, using an iterative Gauss-newton ap-
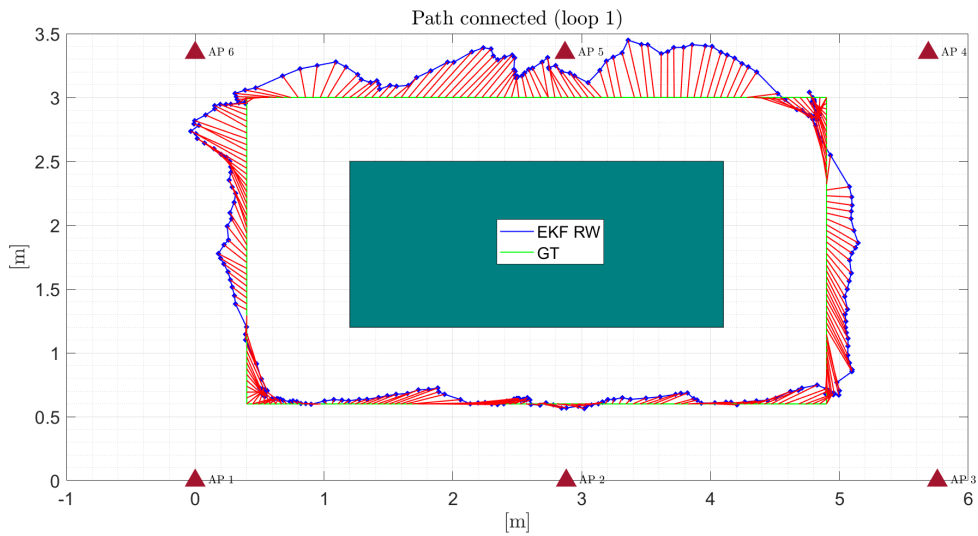
Figure 5.16: Plot of the connected path between the EKF positions and the ground truth for the first loop of the related target.
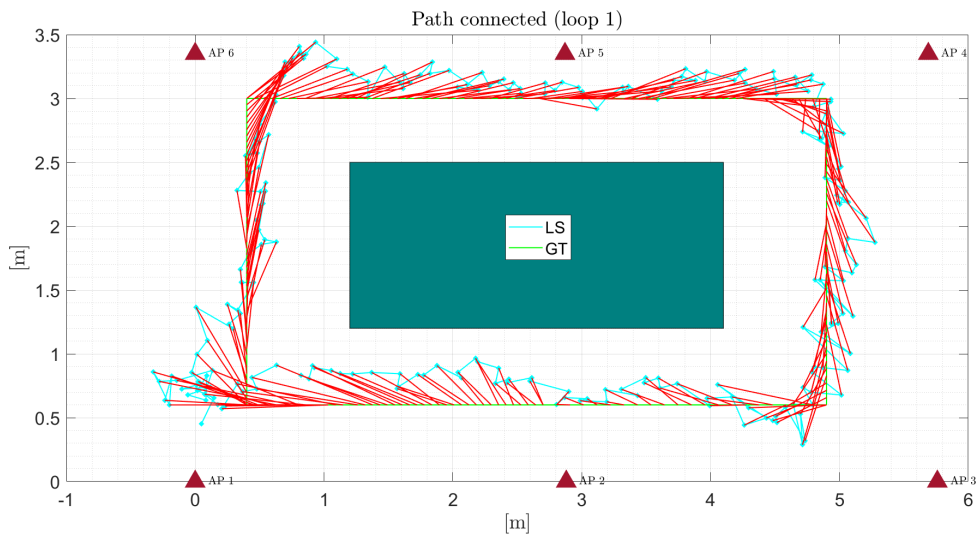
Figure 5.17: Plot of the connected path between the LS positions and the ground truth for the first loop of the related target.

proch:

$$\hat{x}_k = \underset{x}{\arg\min} g(x)^T g(x) \tag{5.13}$$

where the vector g(x) is defined as:

$$g_i(x) = \sqrt{(x - x_i)^2 + (y - y_i)^2} - [\hat{D}]_{ik} \tag{5.14}$$

where x_i is a set of all anchors with known position.

- iterating the process several times, we reach a solution when the error $||g(x)||$ is lower than a fixed threshold, giving as an output the anchor position. Repeating the process for each anchor we can obtain all the anchor's positions.

It is possible to compare the performance of the positioning using as input for the filter the anchor positions computed from the auto-localization of the T4F application and the one corresponding to the real positions of the devices, pre-measured during the experimental campaign. Figure5.19 and Figure5.20 show the path comparison between the two cases for the office experiments for both tag 1 and 2.

It is possible to see that the overall path is not having major issues, if not a little movement of the whole loop, which now appear slightly translated with respect to the other one.

The CDF is also calculated, as seen in Figure5.21 and Figure5.22, with the respective
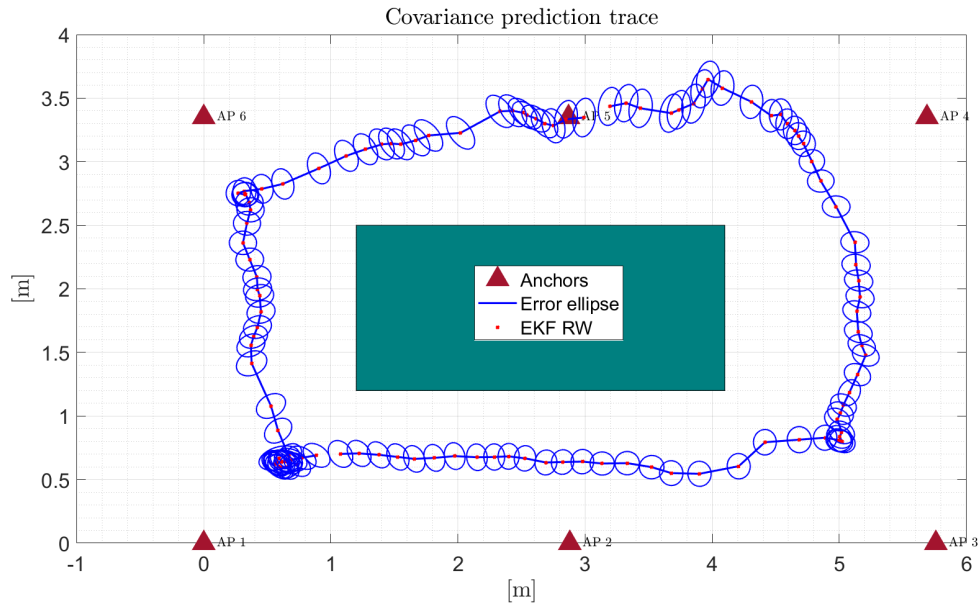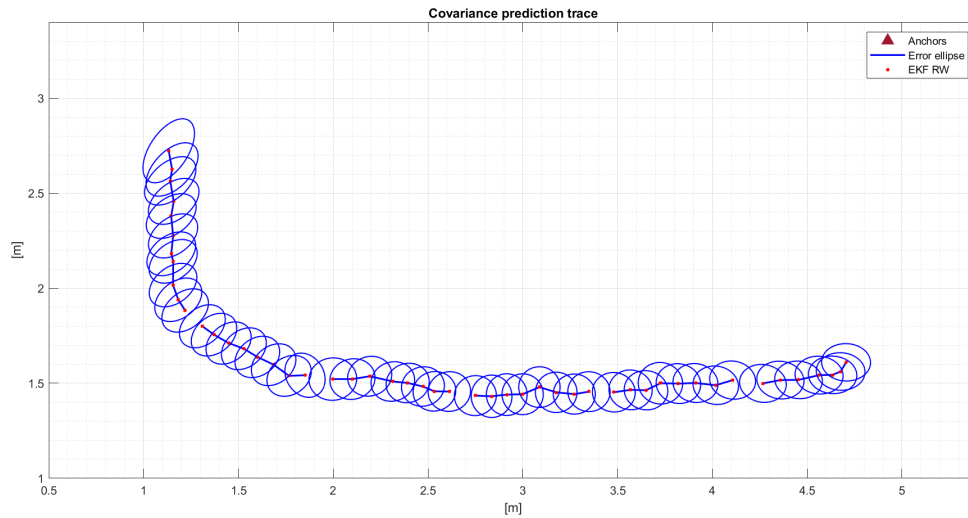

Figure 5.18: Plot of the trace of the prediction covariance for each estimated position of the EKF using the random walk model for the office acquisition, tag 2, first loop.

CEP95 values: For the first tag:

- EKF RW REAL AP: CEP95 = 0.41m

- EKF RW T4F AP: CEP95 = 0.46m

For the second tag we obtain:
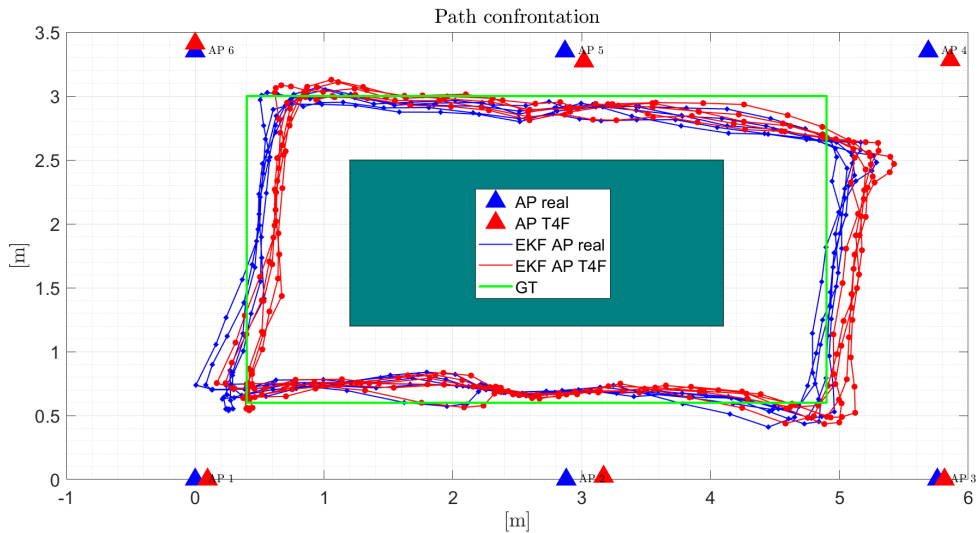
Figure 5.19: Plot of the different path generated from the usage of the real AP positions and the one calculated by the T4F auto-localization algorithm for the tag 1 of the office acquisitions.
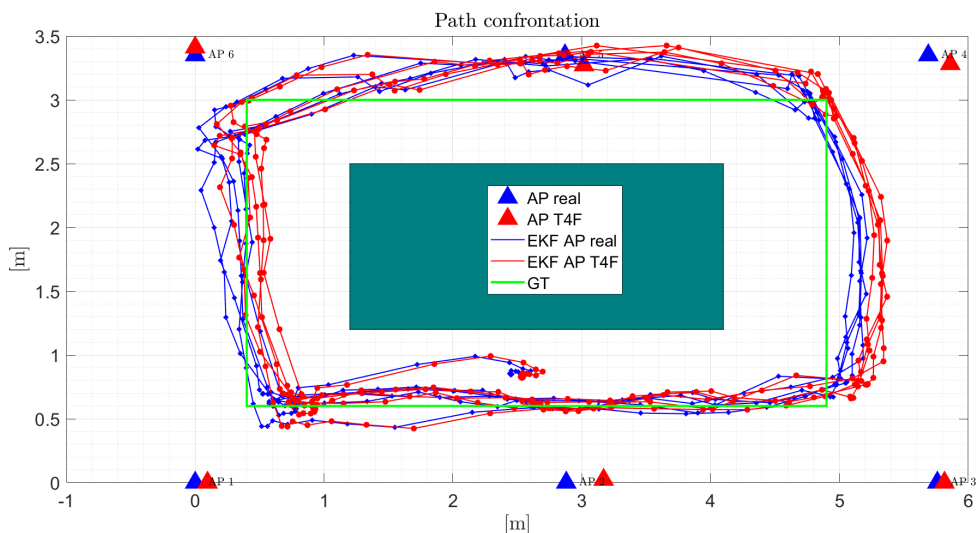
Figure 5.20: Plot of the different path generated from the usage of the real AP positions and the one calculated by the T4F auto-localization algorithm for the tag 2 of the office acquisitions.

- EKF RW REAL AP: CEP95 = 0.48m

- EKF RW T4F AP: CEP95 = 0.53m

The results confirm the fact that with respect to the ground truth, the path computed with the T4F anchors auto-localization provides as a result a slightly worst result with respect to the real position's one. Although the result gives a slight worsening of the performance,
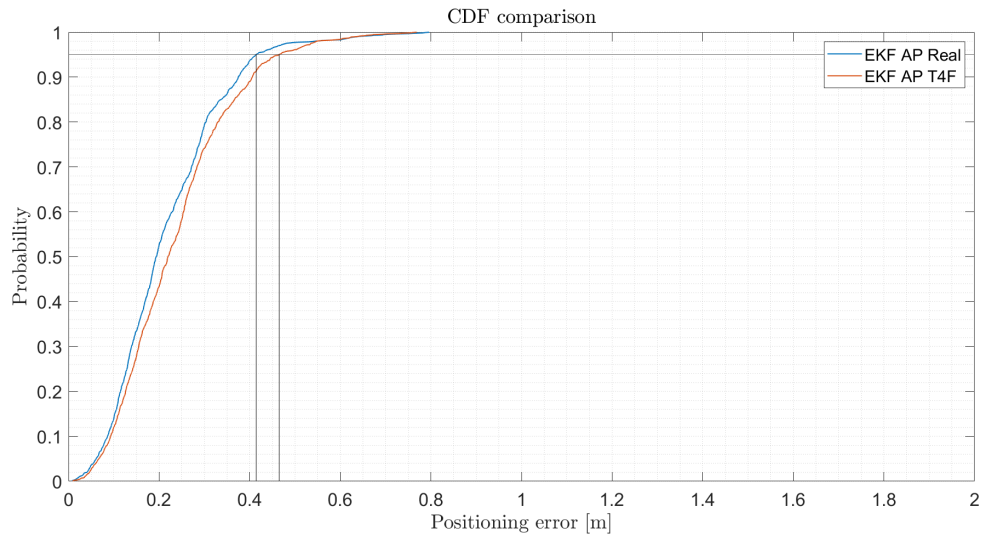
Figure 5.21: Cumulative density function of the position error respectively for the EKF Random walk for the real position of the AsP and the EKF random walk for the T4F auto-localized positions of the APs for tag 1 of the office experiment.
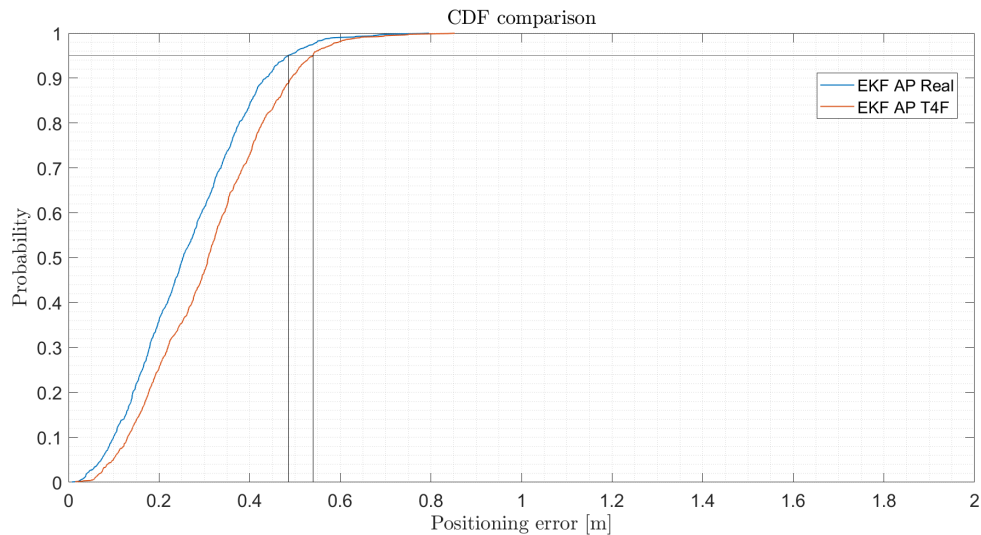
Figure 5.22: Cumulative density function of the position error respectively for the EKF Random walk for the real position of the AsP and the EKF random walk for the T4F auto-localized positions of the APs for tag 2 of the office experiment.

it is still good enough to consider a possible improvement not totally necessary.

5.3.   AGV acquisition analysis

The second experiment consists in analyzing the acquisitions related to the AGV. As shown in the previous sections for the office area, the results are portrayed in three different visualizations: the path comparison, with different methods of tracking, the analysis of the CDFs and the related comparisons between motion models and anchors positions. Since the AGV experiments include two different acquisitions, the division is going to be done considering the results for both of them.

5.3.1.   AGV: motion models confrontation

Also for the AGV acquisitions the motion models confrontation are performed. The goal is to observe possible changes or differences with respect to the other indoor acquisition previously shown in relation to the office experiments and to be able to select the optimal motion model for this experiment too. Figure5.23, 5.24, 5.25 and 5.26, show the different paths regarding the motion models for the first acquisition regarding tag 1 and 2:
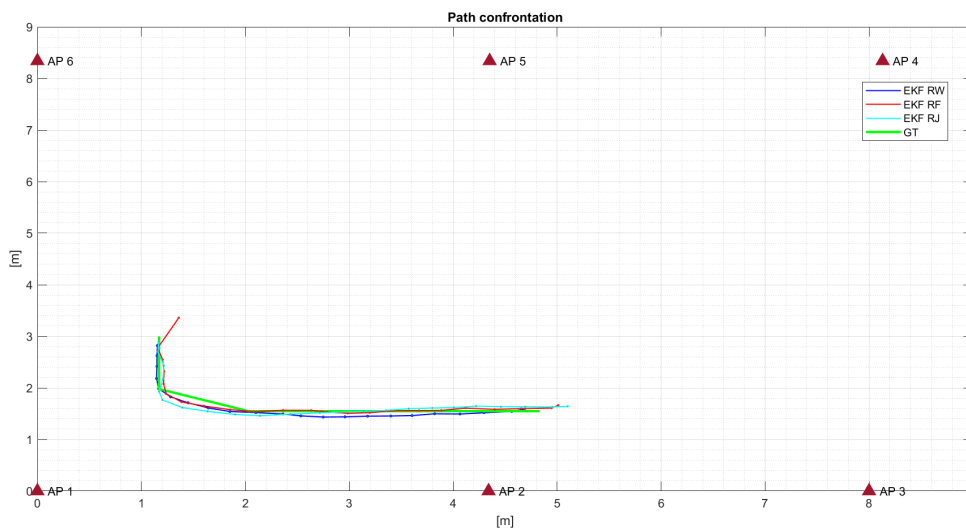
Figure 5.23: Plot of the different motion models path used for the tag 1 of the AGV first acquisition.
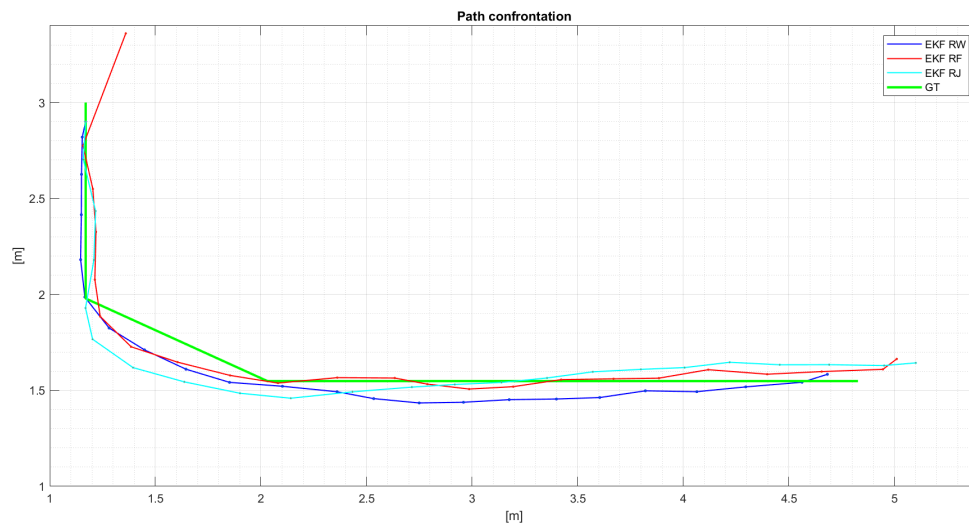
Figure 5.24: Plot of the different motion models path used for the tag 1 of the AGV first acquisition, zoomed in.
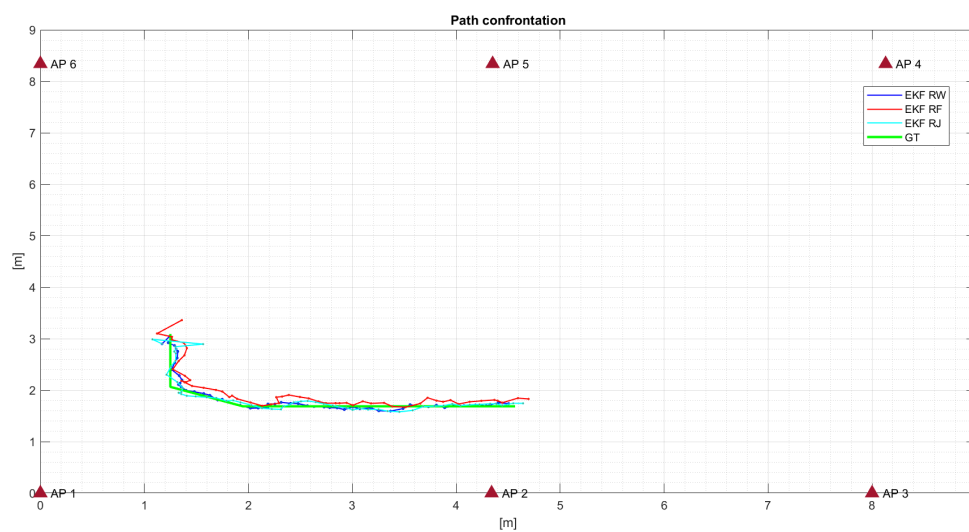
Figure 5.25: Plot of the different motion models path used for the tag 2 of the AGV first acquisition.
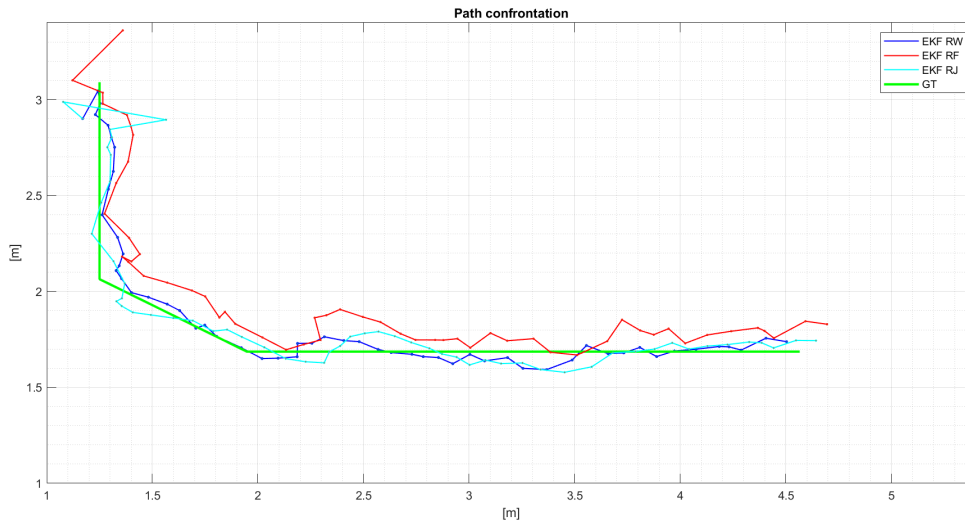
Figure 5.26: Plot of the different motion models path used for the tag 2 of the AGV first acquisition, zoomed in.

It is evident that compared to the office acquisitions the random force model and the random jerk presents better performances. This is mostly due to the fact that the AGV has a near-constant velocity movement, which makes a constant velocity model more suited for the localization. Although this is true, the AGV has a mostly very low velocity observed and the tracking still seem to return good performance also for the random walk model. For what concerns the random jerk model, since the AGV doesn't present any changes of acceleration it is still able to follow the path, but the overall performances will result in a higher error rate and a more confused behaviour during the first stages of the prediction algorithm, presenting a scattered pattern at the beginning of the acquisitions.

The second acquisition of the AGV reguard the second half of the movement of the machine on the pre-decided path (starting from the top right, moving to the bottom middle of the path). In Figure5.27, 5.28,5.29 and 5.30, the path confrontations are showed:
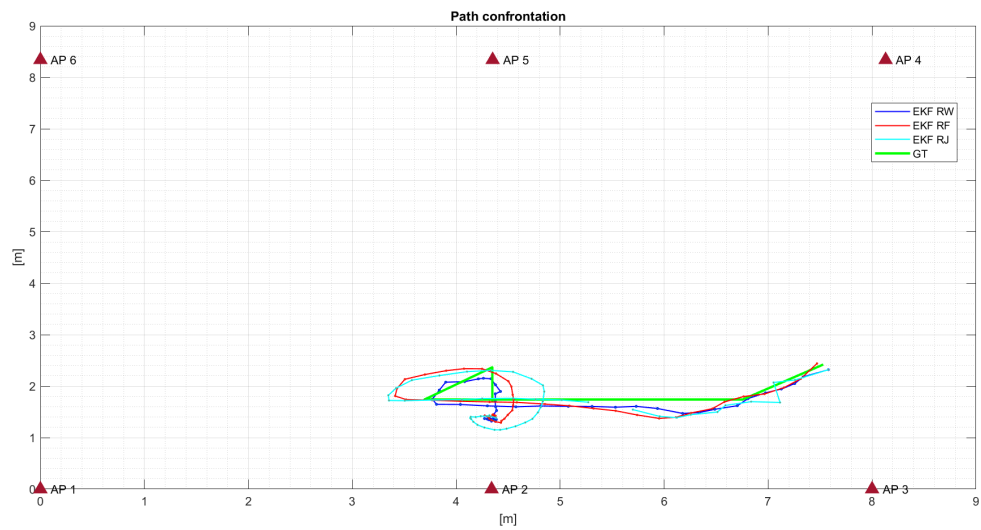
Figure 5.27: Plot of the different motion models path used for the tag 1 of the AGV's second acquisition.
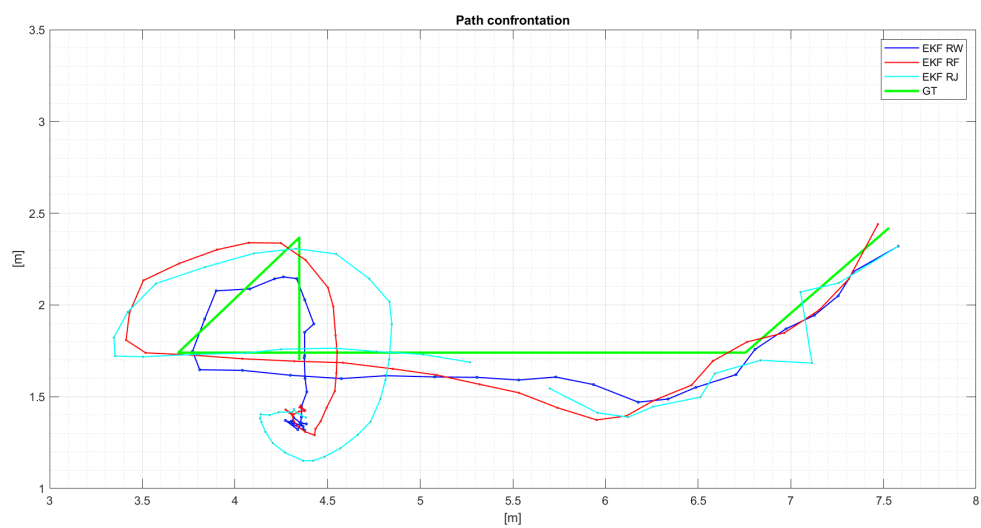
Figure 5.28: Plot of the different motion models path used for the tag 1 of the AGV's second acquisition, zoomed in.
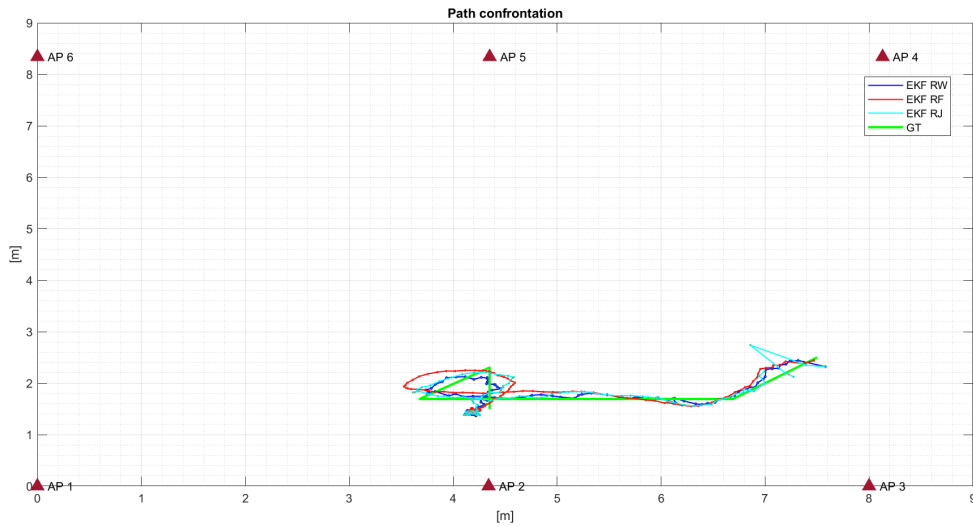
Figure 5.29: Plot of the different motion models path used for the tag 2 of the AGV's second acquisition.
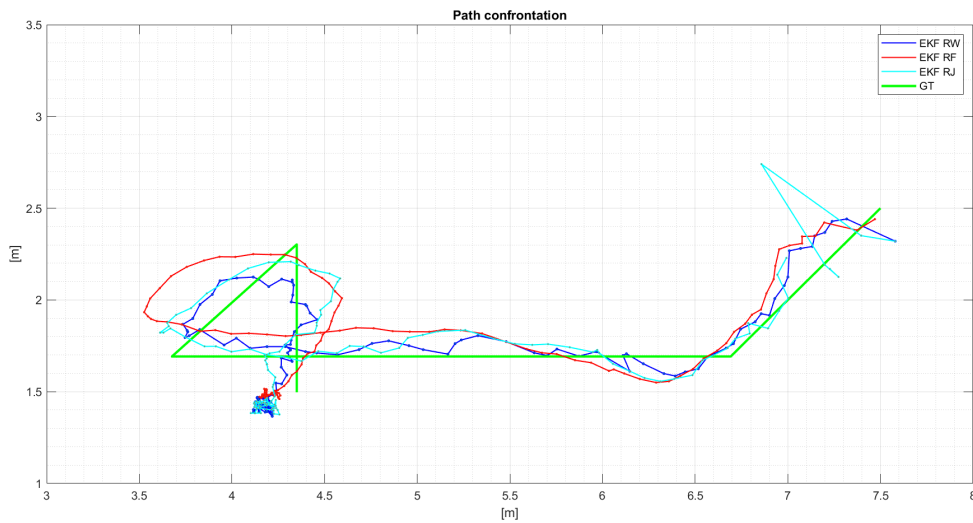
Figure 5.30: Plot of the different motion models path used for the tag 2 of the AGV's second acquisition, zoomed in.

The path presents similarities with the one of the first acquisition, but in this case it is more evident the different behaviour of the models in the curved part of the trajectory. The random force and random jerk model presents a larger curvature with respect to the random walk result.

The CDF results, in Figure5.31 and 5.32 for the first acquisition respectively for tag 1 and 2, and Figure5.33 and 5.34 for the second acquisition tag 1 and 2, provides some more detail about the actual estimated positioning error:
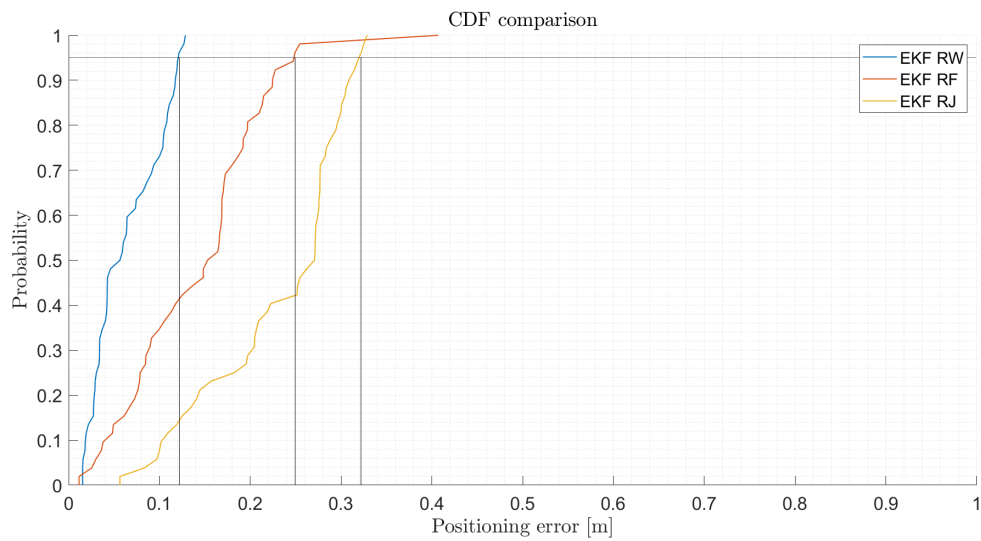
Figure 5.31: Cumulative density function of the position error for the first acquisition of the AGV experiments, tag 1. Respectively are reported the CDF for the EKF Random walk, EKF random force and EKF random jerk model positions compared to the ground truth.
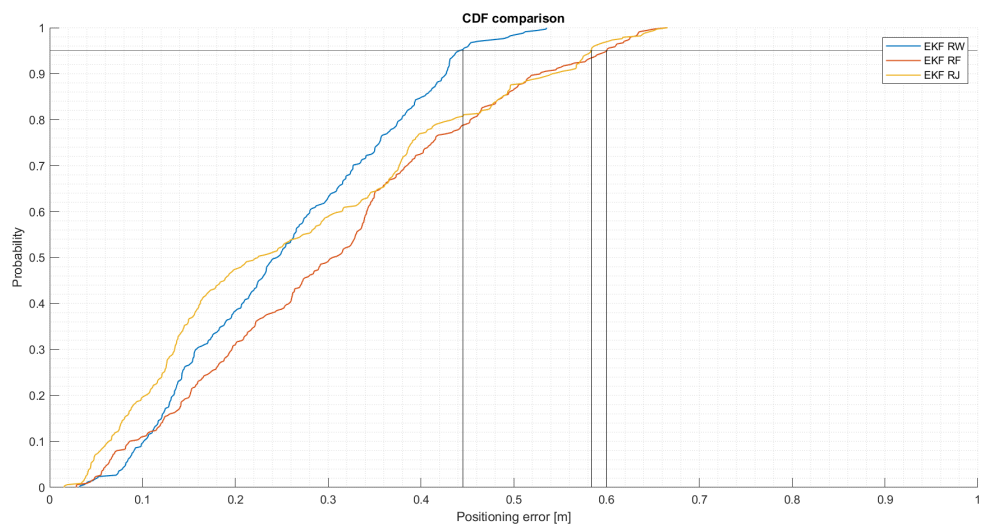
Figure 5.32: Cumulative density function of the position error for the first acquisition of the AGV experiments, tag 2. Respectively are reported the CDF for the EKF Random walk, EKF random force and EKF random jerk model positions compared to the ground truth.

For the tag 1 the CEP95 values are the following:

- EKF RW: CEP95 = 0.13m

- EKF RF: CEP95 = 0.25m

- EKF RJ: CEP95 = 0.33m

For the second tag we obtain:

- EKF RW: CEP95 = 0.44m

- EKF RF: CEP95 = 0.6m

- EKF RJ: CEP95 = 0.58m
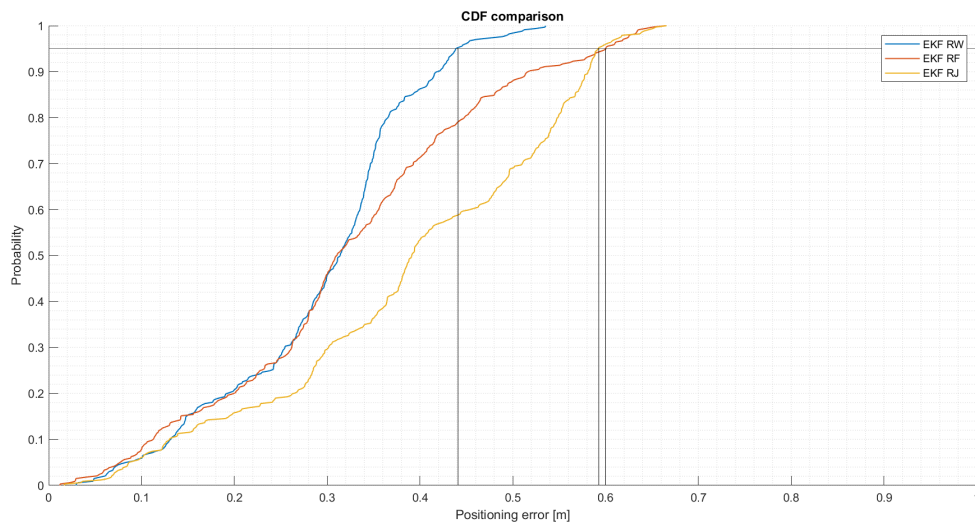
Figure 5.33: Cumulative density function of the position error for the second acquisition of the AGV experiments, tag 1. Respectively are reported the CDF for the EKF Random walk, EKF random force and EKF random jerk model positions compared to the ground truth.
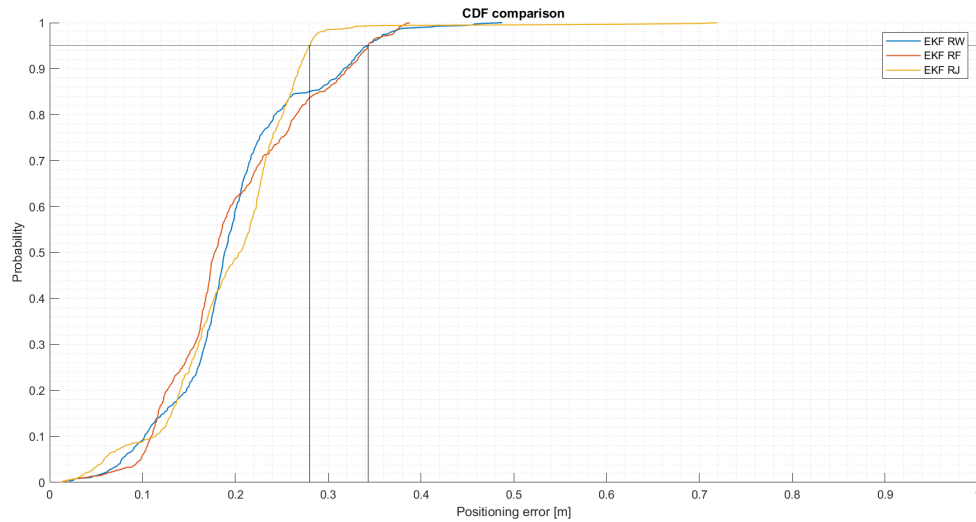
Figure 5.34: Cumulative density function of the position error for the second acquisition of the AGV experiments, tag 2. Respectively are reported the CDF for the EKF Random walk, EKF random force and EKF random jerk model positions compared to the ground truth.

For the tag 1 the CEP95 values are the following:

- EKF RW: CEP95 = 0.44m

- EKF RF: CEP95 = 0.6m

- EKF RJ: CEP95 = 0.59m

For the second tag we obtain:

- EKF RW: CEP95 = 0.34m

- EKF RF: CEP95 = 0.34m

- EKF RJ: CEP95 = 0.28m

It is interesting to see how reduced the errors for the random force and random jerk model are with respect to the office acquisitions. This provides a better understanding and proof of how the motion models can adapt to the specific target's movement behaviour. Nonetheless, the better overall performance of the random walk model is still leading us to the selection of that model for the other confrontations.

5.3.2. AGV: acquisition 1 results

The first acquisition is the one regarding the first part of the path computed by the AGV including the left side of the pre-calculated path for the device. Figure5.35 and 5.36 provides for the first tag, the path difference between the Extended Kalman filter using random walk model, the LS algorithm and the T4F raw data extracted from the related application. The three paths have different behaviour: The EKF path is actually tracking the movement of the tag showing a more linear path following the Ground truth line. The LS is instead quite scattered along the same path, showing how the tracking is not being

Figure 5.35: Path difference of the AGV acquisition for tag 1. Highlighted EKF with a random walk model, LS algorithm and estimated ground truth path.

Figure 5.36: Path difference of the AGV acquisition for tag 1. Highlighted EKF with a random walk model, LS algorithm and estimated ground truth path. Zoomed in version.

performed. The T4F results, although following a smooth line are too filtered and results in a very approximated shape.

Analyzing the CDF of each position error, shown in Figure5.37, we can extract the CEP95 data, providing the localization error of each path with respect to the ground truth. As the previous experiments the LS and the extracted data from T4F are performing worse than the filtered ones with the EKF. The following CEP95 values are calculated:

- EKF RW: CEP95 = 0.41m

- EKF RF: CEP95 = 0.77m

- EKF RJ: CEP95 = 1.03m

The representation shown in Figure5.38 (for the EKF) and Figure5.39 (for the LS), is also providing a visual proof of how the filter is helping with the tracking with respect to the LS visualization:

Figure 5.37: Cumulative density function of the position error respectively for the EKF, LS algorithm and T4F raw data compared to the ground truth for tag 1
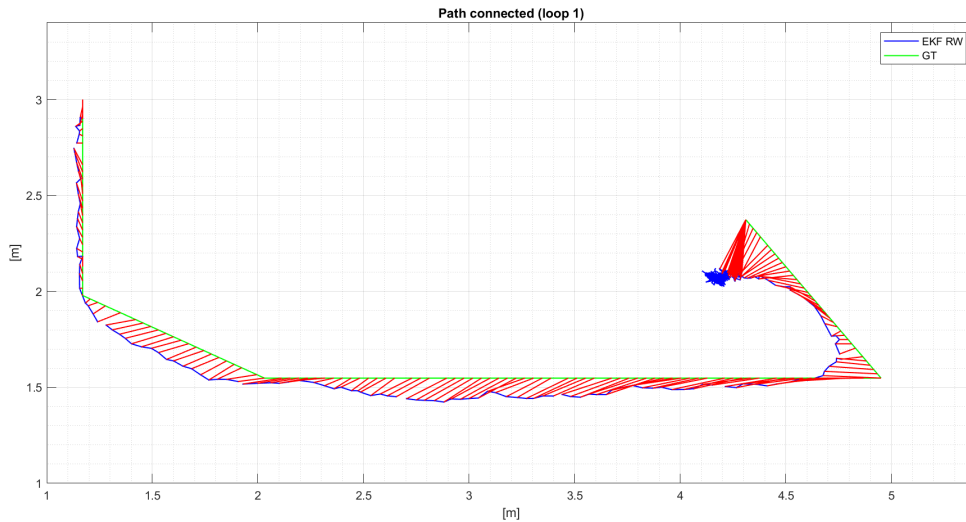
Figure 5.38: Plot of the connected path between the EKF positions and the ground truth for the AGV acquisition, tag 1.
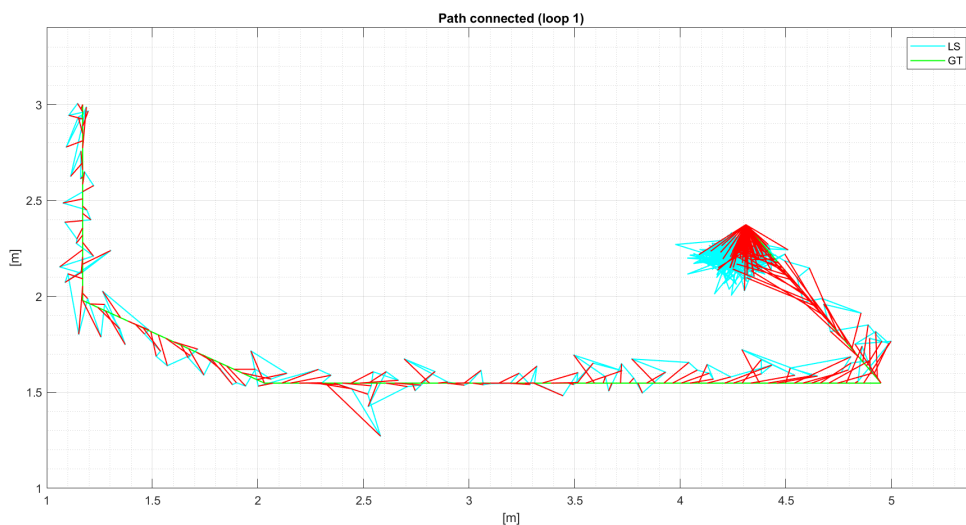
Figure 5.39: Plot of the connected path between the LS positions and the ground truth for the AGV acquisition, tag 1.

The connected path highlight the scattered behaviour of the LS algorithm with respect to the tracking nature of the EKF filtering.

The trace of prediction covariance representation is also reported in Figure5.40: The picture highlight how the error is incredibly small over all the path.

The results for the second tag are now presented: First the different paths, highlighting the EKF, LS and T4F raw data comparison, visualized in Figure5.41:

Figure 5.40: Plot of the trace of the prediction covariance for each estimated position of the EKF using the random walk model for the AGV acquisition 1, tag 1
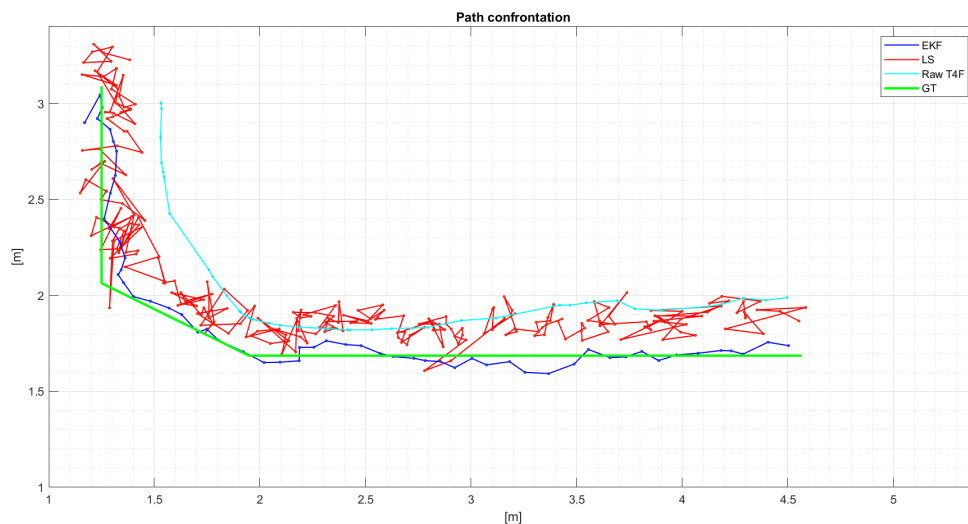
Figure 5.41: Path difference of the AGV acquisition for tag 1. Highlighted EKF with a random walk model, LS algorithm and estimated ground truth path.

Also in this case the results presents similarities with the previous one, showing a better performance of the EKF with respect to the other methodologies, which hardly follows the ground truth path in a satisfying way, presenting approximations and scattered position tracking compared to the filtering solution.

As reported in Figure5.42, The CDF plot also show similarities with the tag 1.

- EKF RW: CEP95 = 0.44m

- EKF RF: CEP95 = 0.76m
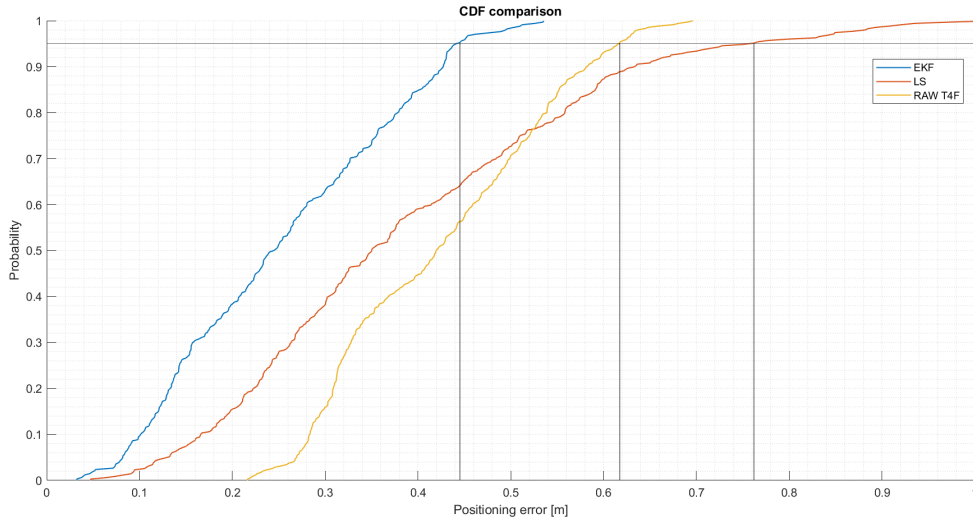
Figure 5.42: Cumulative density function of the position error respectively for the EKF, LS algorithm and T4F raw data compared to the ground truth for tag 2
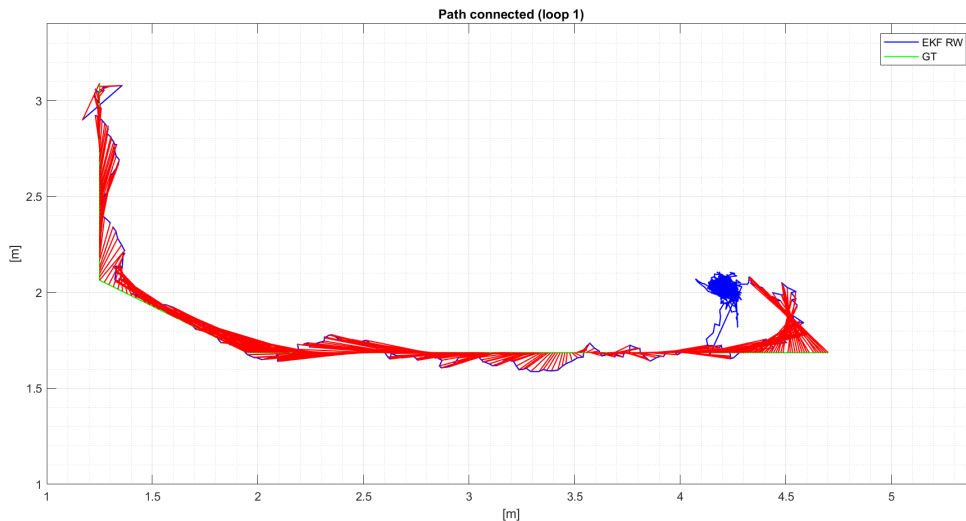
Figure 5.43: Plot of the connected path between the EKF positions and the ground truth for the AGV acquisition, tag 2.

- EKF RJ: CEP95 = 0.61m

Even though the EKF is still performing the best, the T4F data results are surprisingly showing a better error than the LS counterpart. This may be due to the highly scattered nature of the LS positions, which are also shown in the connected path visualization as presented in Figure5.43 (for the EKF) and Figure5.44 (for the LS):

The trace of the prediction covariance is presented as in Figure5.45: As expected the second tag is performing slightly worse than the first one, visible trough the stretched ellipses along the path.
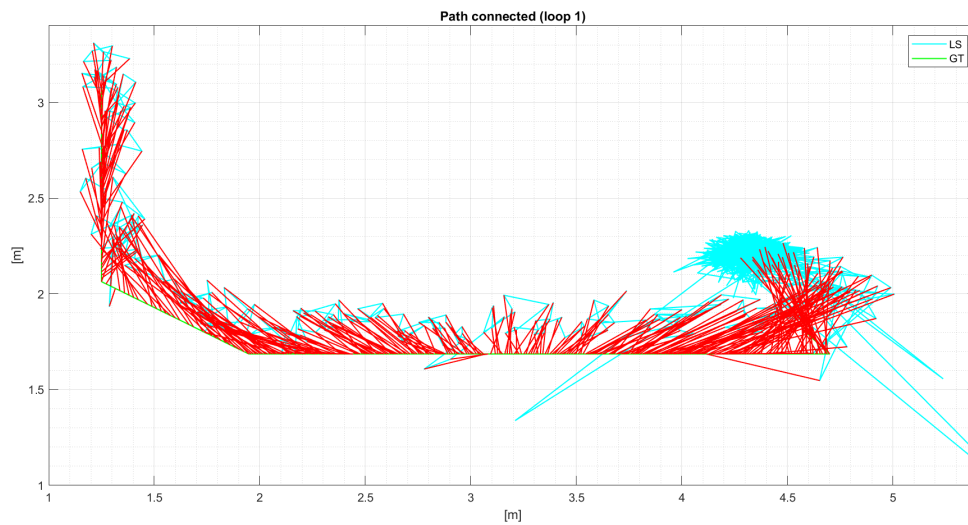
Figure 5.44: Plot of the connected path between the LS positions and the ground truth for the AGV acquisition, tag 2.
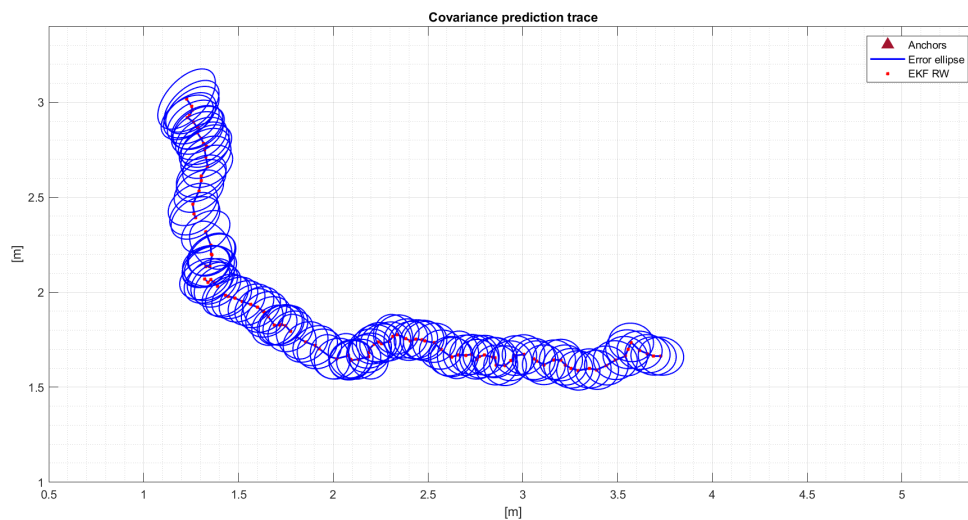
Figure 5.45: Plot of the trace of the prediction covariance for each estimated position of the EKF using the random walk model for the AGV acquisition 1, tag 1

5.3.3. AGV: acquisition 2 results

The second acquisition of the AGV follows the second part of the path, starting from the top right, going down to the middle and then turning on itself to get parked right at the bottom of the path. The following results add up to the previous one to ensure the effectiveness of the EKF filtering over the other techniques, starting with the path comparison for tag 1, shown in Figure5.46 and 5.47:
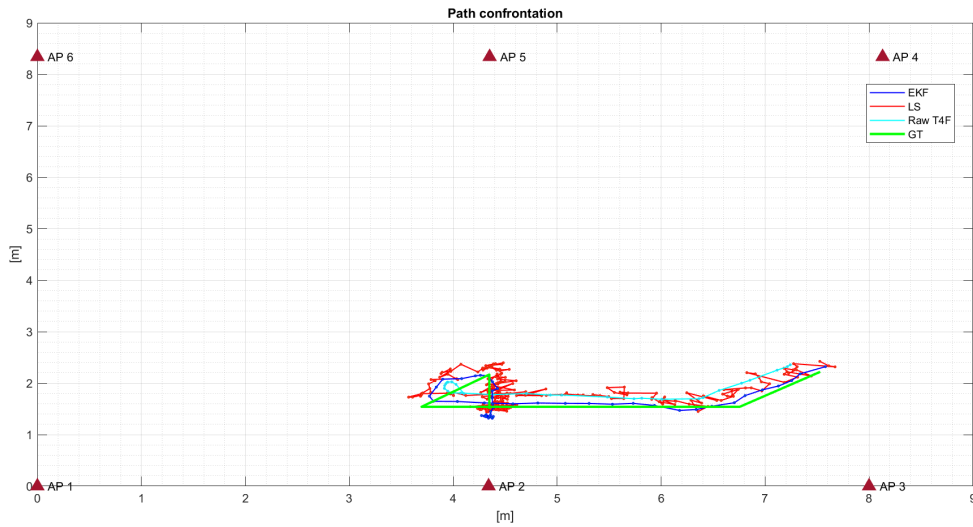
Figure 5.46: Path difference of the AGV's second acquisition for tag 1. Highlighted EKF with a random walk model, LS algorithm and estimated ground truth path.
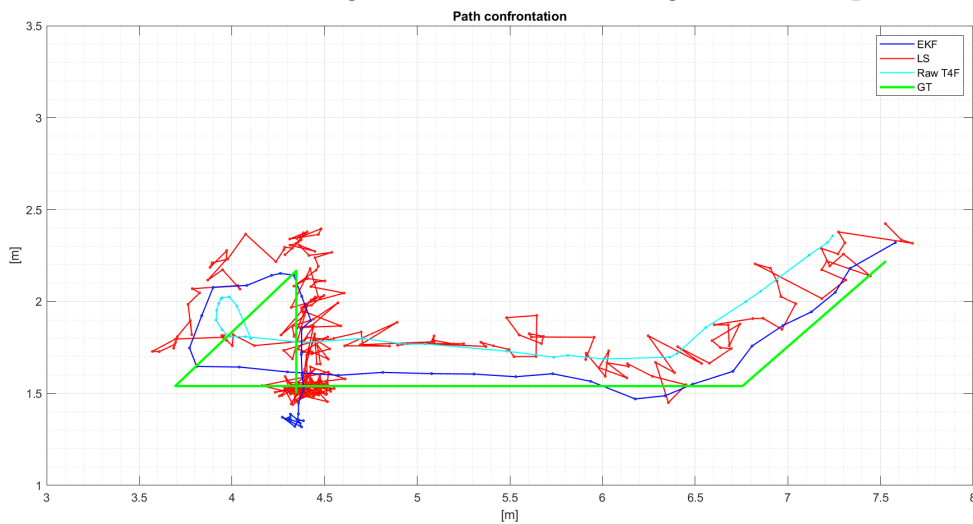
Figure 5.47: Path difference of the AGV's second acquisition for tag 1. Highlighted EKF with a random walk model, LS algorithm and estimated ground truth path. Zoomed in version.

The path is yet again presenting a smoother track for the Kalman filter's position, while the LS is presenting a scattered path and the T4F data are approximating the trajectory to a fast turn on the curved side. The CEP95 computed through the CDF calculation showed in Figure5.48 for the first tag:
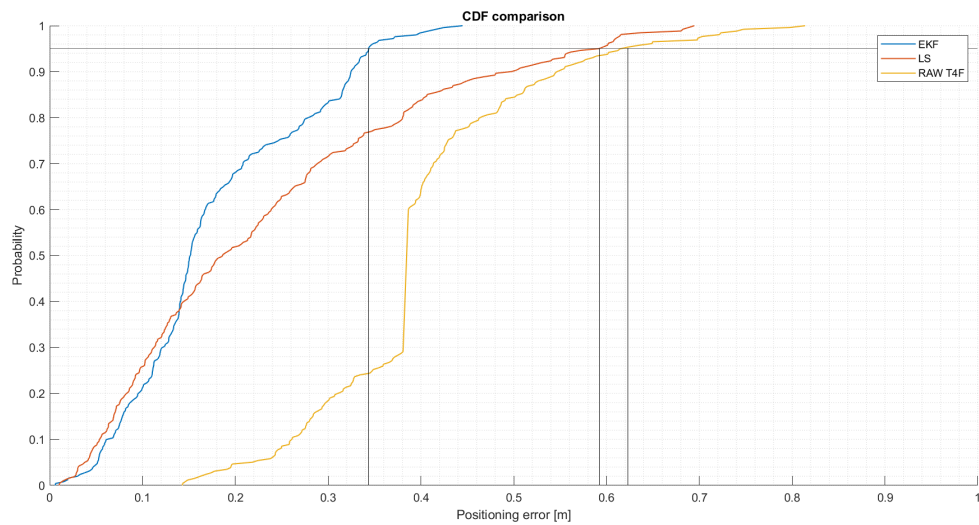
Figure 5.48: Cumulative density function of the position error respectively for the EKF, LS algorithm and T4F raw data compared to the ground truth for tag 1

- EKF RW: CEP95 = 0.35m

- EKF RF: CEP95 = 0.37m

- EKF RJ: CEP95 = 0.46m

The trend is the same as the other acquisitions, although all of the results presents a good performance, the EKF is still the one with a lower positioning error.

The same results are now showed for the second tag. Tge path comparison are presented in Figure5.49 and Figure5.50.
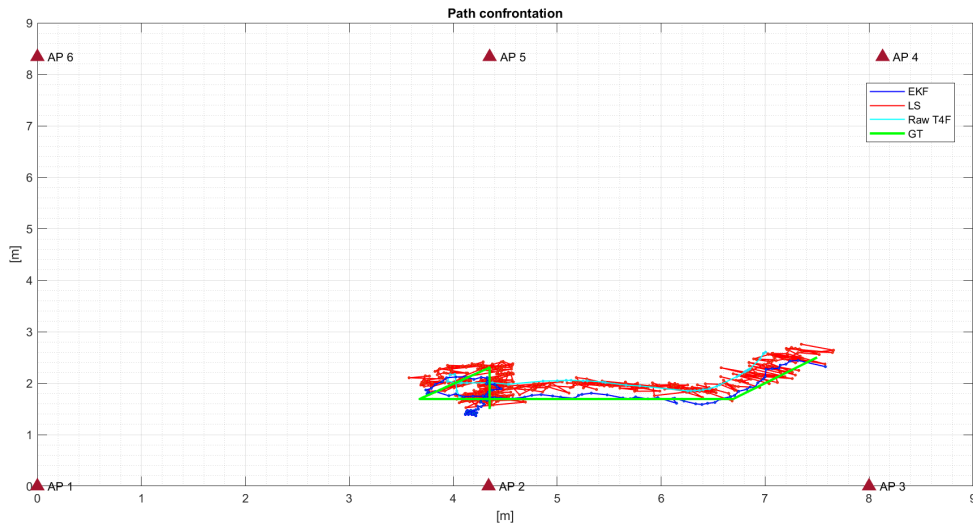
Figure 5.49: Path difference of the AGV's second acquisition for tag 1. Highlighted EKF with a random walk model, LS algorithm and estimated ground truth path.
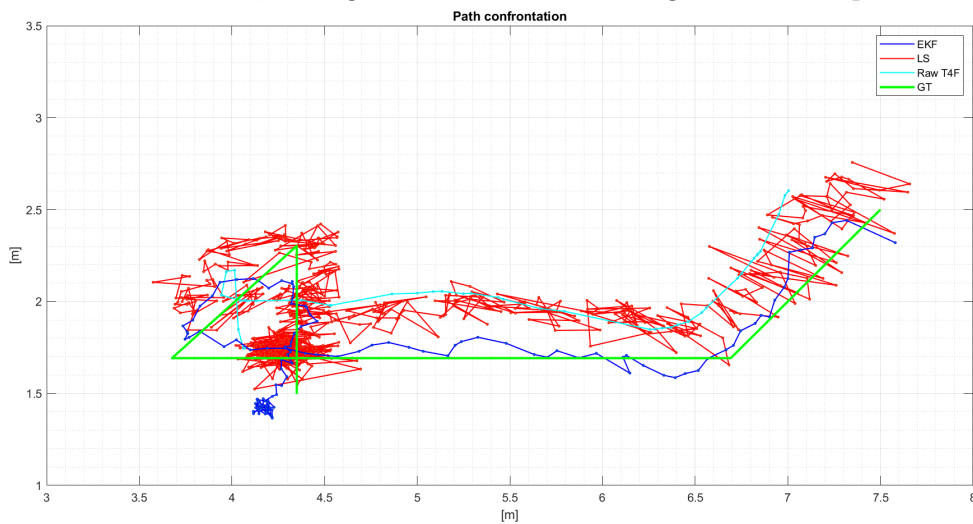
Figure 5.50: Path difference of the AGV's second acquisition for tag 1. Highlighted EKF with a random walk model, LS algorithm and estimated ground truth path. Zoomed in version.

Even though the type of behaviour of the three positioning methods are the same, we can easily observe a much worse behaviour in the scattering positions registered by the LS algorithm. The CEP95 computed trough the CDF calculation in Figure5.51:
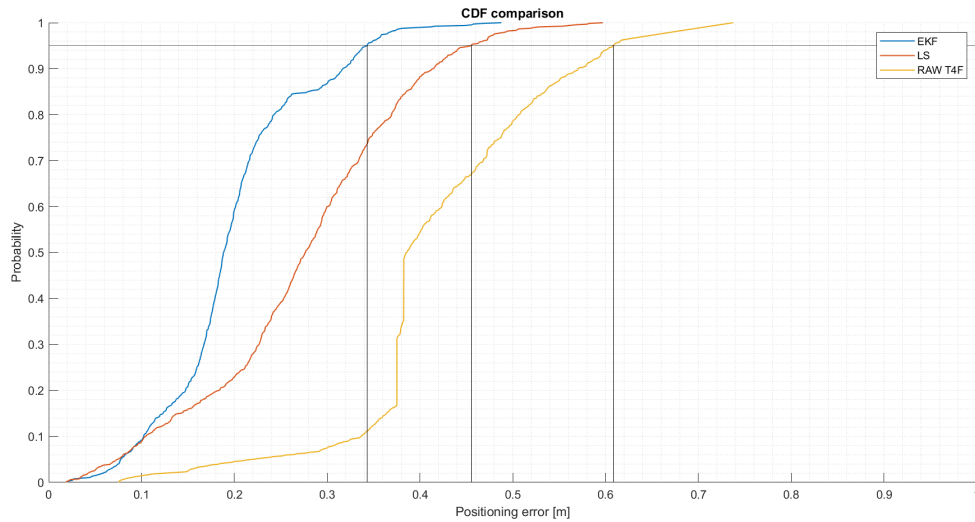
Figure 5.51: Cumulative density function of the position error respectively for the EKF, LS algorithm and T4F raw data compared to the ground truth for tag 1

- EKF RW: CEP95 = 0.34m

- EKF RF: CEP95 = 0.45m

- EKF RJ: CEP95 = 0.60m

As stated before the filter improves the performance in every iteration.

5.3.4. AGV: anchors position confrontation

The anchors auto-localization is also tested for the AGV results. The pictures in Figure5.52 and 5.53, highlight the path difference for the first acquisition of the AGV experiments for tag 1 computed with the EKF random walk for the real anchors positions and the one provided by the T4F algorithm:
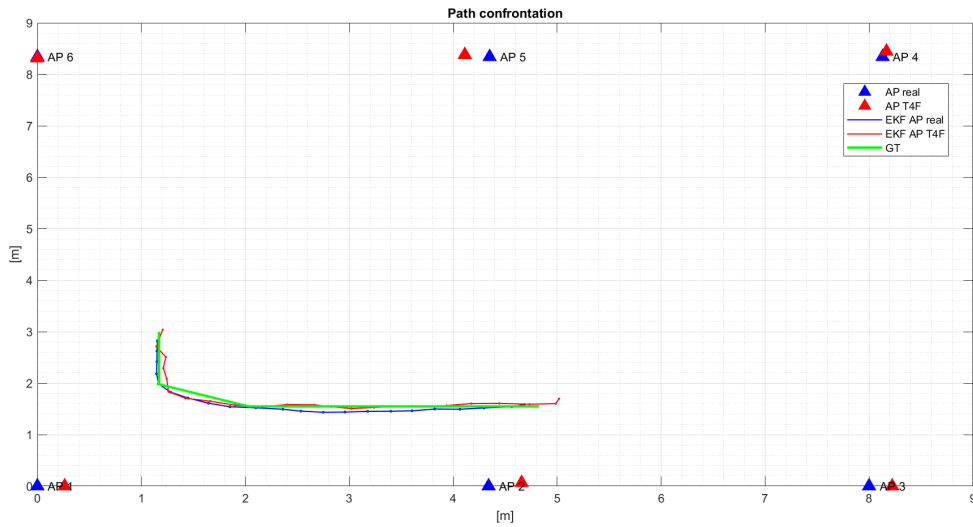
Figure 5.52: Plot of the different path generated from the usage of the real AP positions and the one calculated by the T4F auto-localization algorithm for the tag 1 of the AGV's first acquisition.
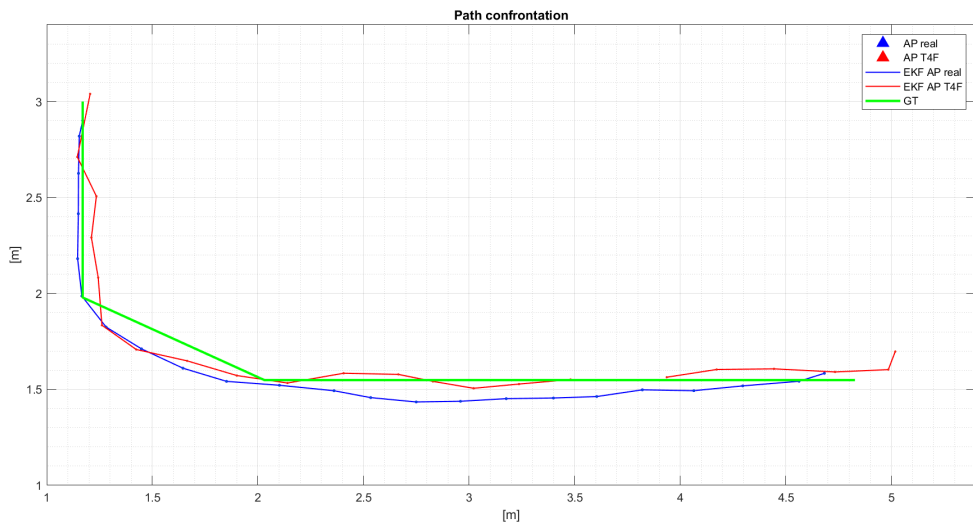
Figure 5.53: Plot of the different path generated from the usage of the real AP positions and the one calculated by the T4F auto-localization algorithm for the tag 1 of the AGV's first acquisition, zoomed in.

For the second acquisition, we get the results shown in Figure5.54 and 5.55 for tag 1, and Figure5.56 and 5.57 for tag 2:
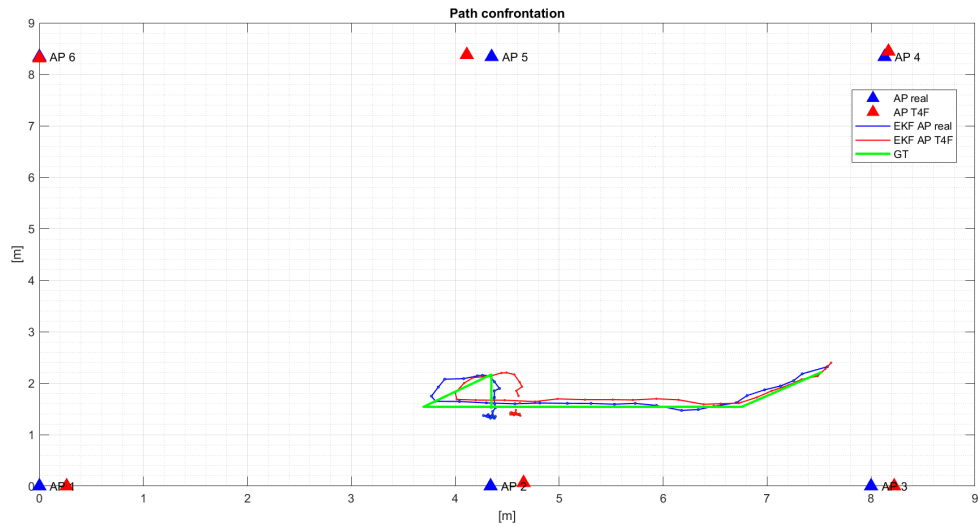
Figure 5.54: Plot of the different path generated from the usage of the real AP positions and the one calculated by the T4F auto-localization algorithm for the tag 1 of the AGV's second acquisition.
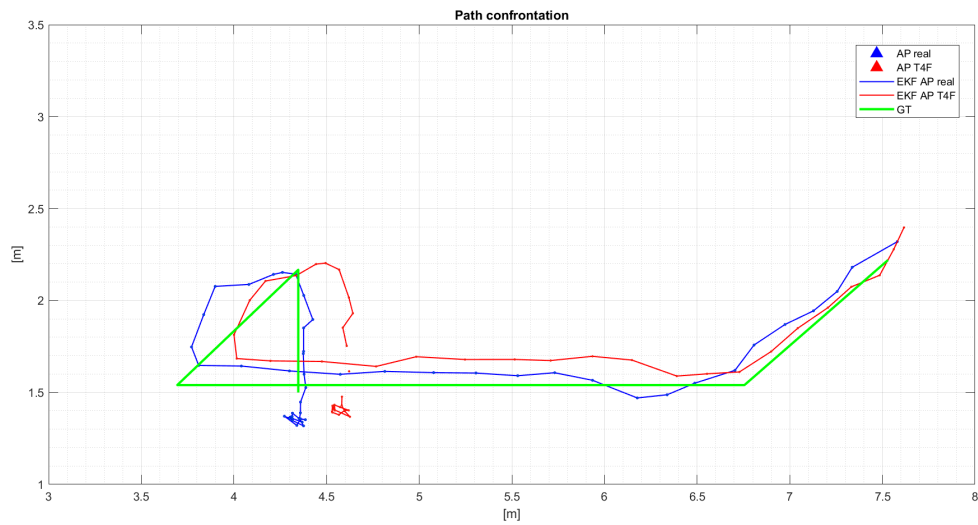
Figure 5.55: Plot of the different path generated from the usage of the real AP positions and the one calculated by the T4F auto-localization algorithm for the tag 1 of the AGV's second acquisition, zoomed in.
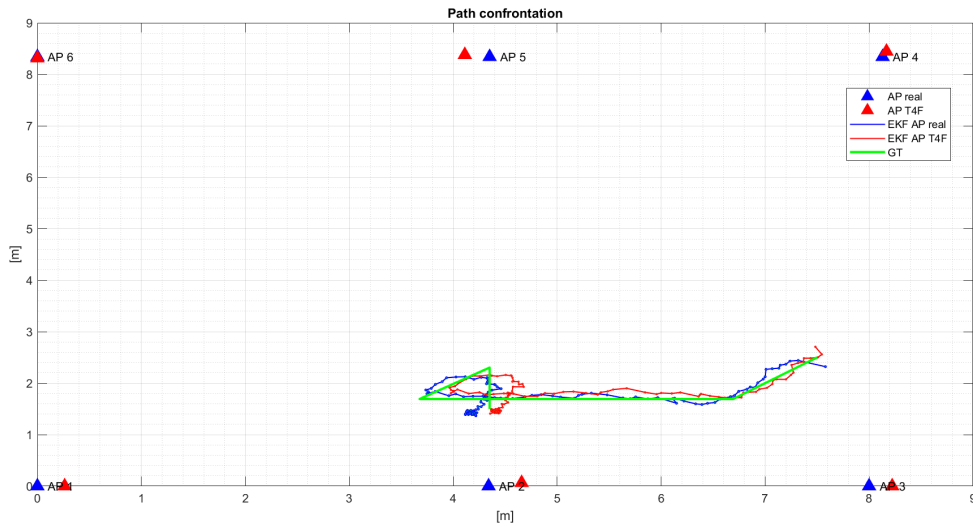
Figure 5.56: Plot of the different path generated from the usage of the real AP positions and the one calculated by the T4F auto-localization algorithm for the tag 2 of the AGV's second acquisition.
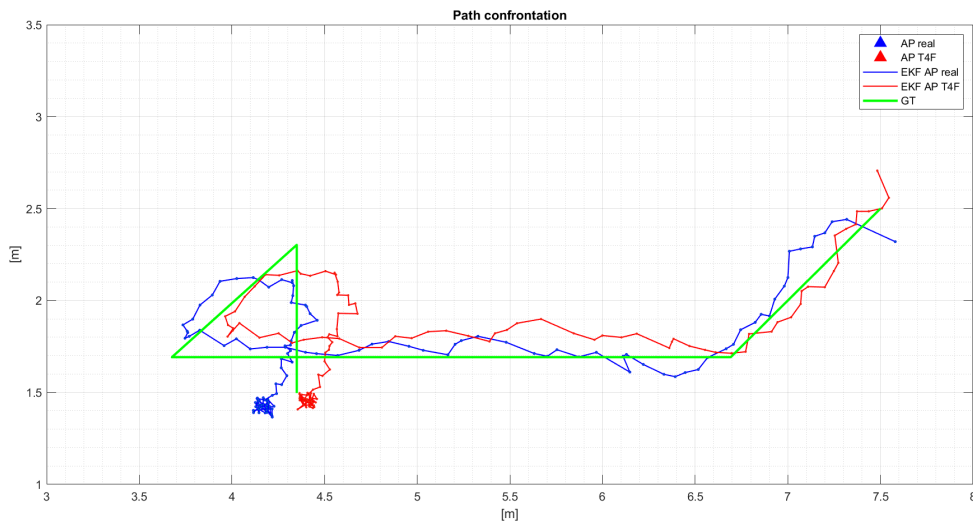
Figure 5.57: Plot of the different path generated from the usage of the real AP positions and the one calculated by the T4F auto-localization algorithm for the tag 2 of the AGV's second acquisition, zoomed in.

Just like in the office acquisition, the overall path is not having major issues, if not a little movement of the whole path, which now appear slightly translated with respect to the other one.

The CDF is also calculated, as shown in Figure5.58 for tag 1 and Figure5.59 for tag 2 of the first acquisition, with the respective CEP95 values:
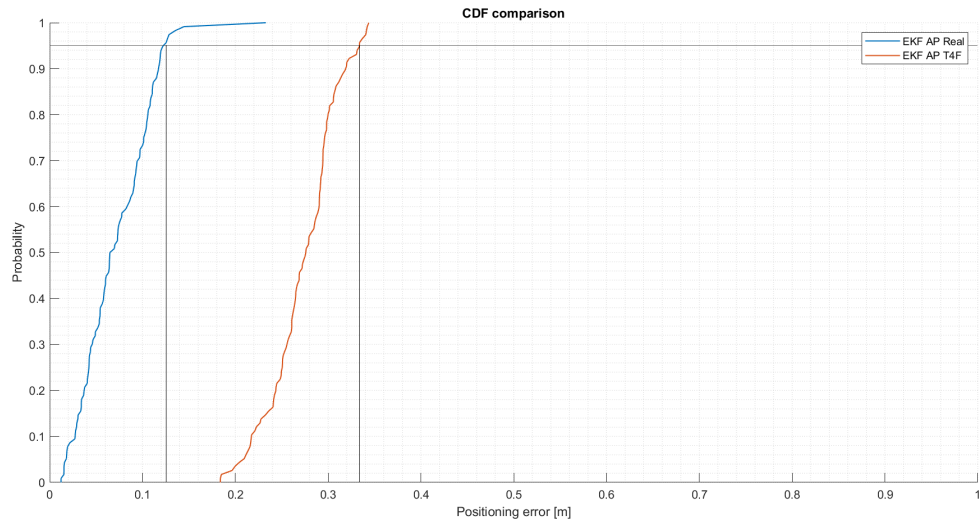
Figure 5.58: Cumulative density function of the position error respectively for the EKF Random walk for the real position of the AsP and the EKF random walk for the T4F auto-localizated positions of the APs for tag 1 of the AGV's first acquisition.
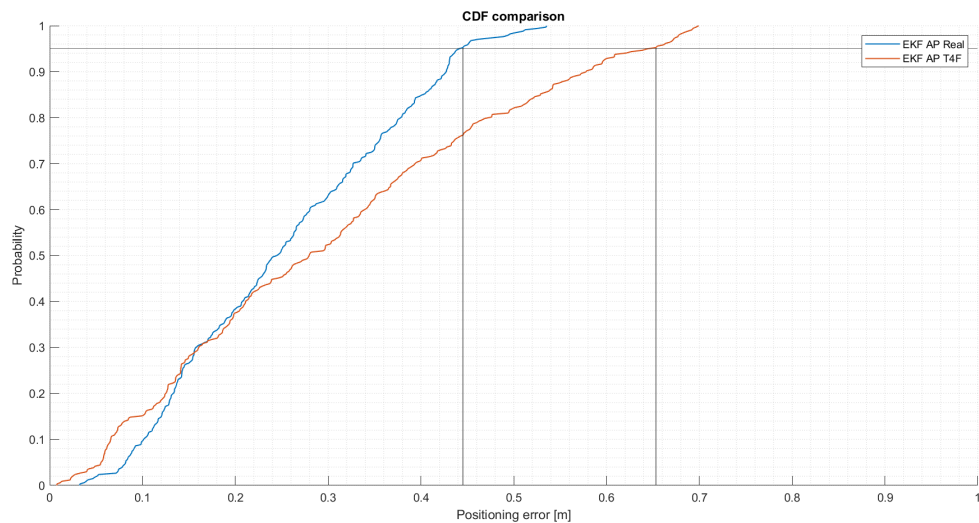
Figure 5.59: Cumulative density function of the position error respectively for the EKF Random walk for the real position of the AsP and the EKF random walk for the T4F auto-localizated positions of the APs for tag 2 of the AGV's first acquisition.

For the first tag:

- EKF RW REAL AP: CEP95 = 0.13m

- EKF RW T4F AP: CEP95 = 0.33m

For the second tag we obtain:

- EKF RW REAL AP: CEP95 = 0.44m

- EKF RW T4F AP: CEP95 = 0.65m

For the second acquisitions, the results are shown in Figure5.60 for the first tag and Figure5.61 for the second tag: For the first tag:

- EKF RW REAL AP: CEP95 = 0.35m
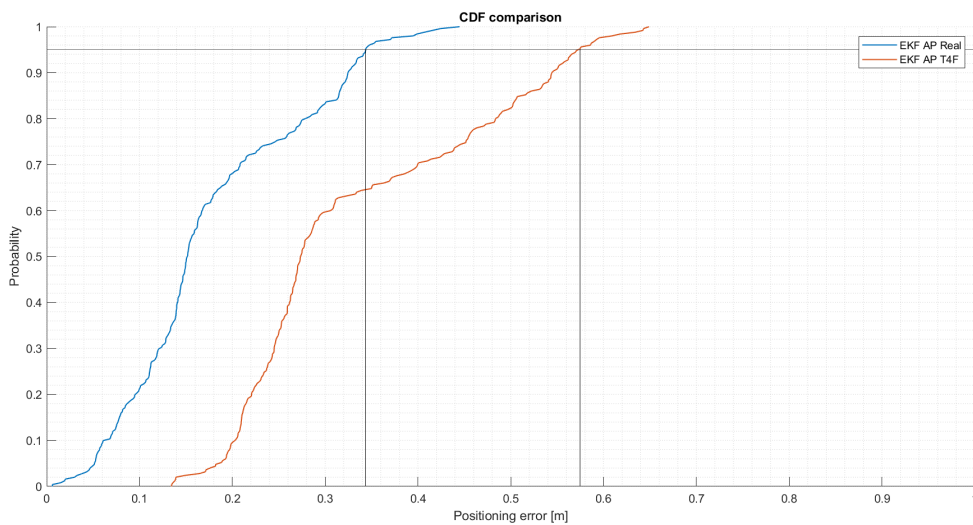
Figure 5.60: Cumulative density function of the position error respectively for the EKF Random walk for the real position of the AsP and the EKF random walk for the T4F auto-localizated positions of the APs for tag 1 of the AGV's second acquisition.
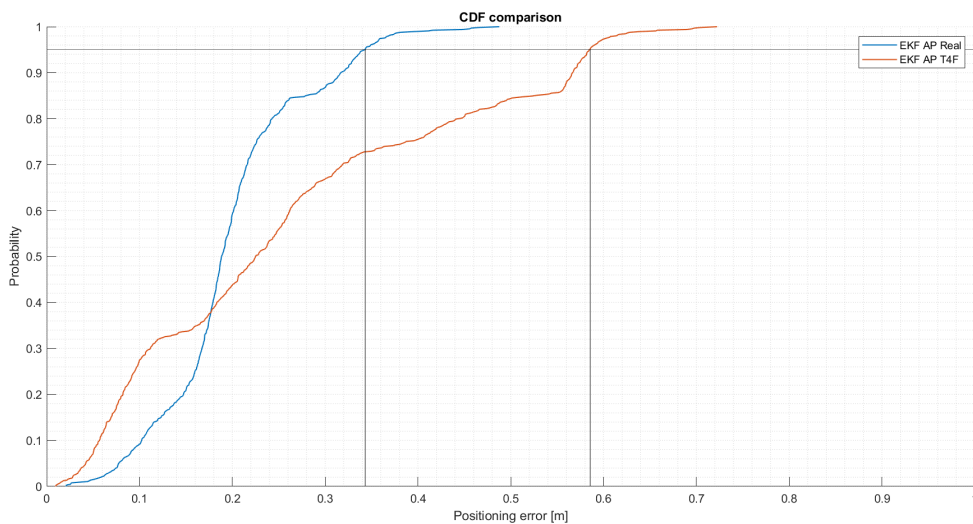
Figure 5.61: Cumulative density function of the position error respectively for the EKF Random walk for the real position of the AsP and the EKF random walk for the T4F auto-localizated positions of the APs for tag 2 of the AGV's second acquisition.

- EKF RW T4F AP: CEP95 = 0.49m

For the second tag we obtain:

- EKF RW REAL AP: CEP95 = 0.34m

- EKF RW T4F AP: CEP95 = 0.58m

Also in this case the results confirm the expected behaviour in which we obtain higher error with respect to the ground truth for the auto-localized acquisitions.

5.4.   Outdoor acquisition analysis: volleyball field

As mentioned in Section 4.3.2, the measurements obtained for the outdoor acquisitions have some main issues concerning a missing data problem. Testing the acquisitions with the EKF, the obtained results showed many missing spaces, consequently giving an anomaly on the calculated positioning error. The error presented such high values (more than 1 meter) also due to the non coordination of the positioning result to the related ground truth. The loss of some clusters of measurements around specific areas made the reconstruction of the path trough the filtering process faulty and the comparison with a generated ground truth impossible. Figure 5.62, 5.63, 5.64 and 5.65 show the evolution for each sample (made each 10ms) of the TDoA measurements for all the proposed tags. The used tags are tag 3, 4, 6 and 11, which are the one used for the localization of the person in motion. The other tags were used to be static to allow us to estimate the error on the measurements, as shown in Section 4.3.2. The pictures highlight how for each AP used (excluding the second one, which was used as master anchor), the measurement value floated, depending on the position of the target to localize, but some areas remained blank due to the presence of missing data. This means that the majority of the measurements for each anchor in that area presented a NaN result, and had to be discarded for any future analysis.
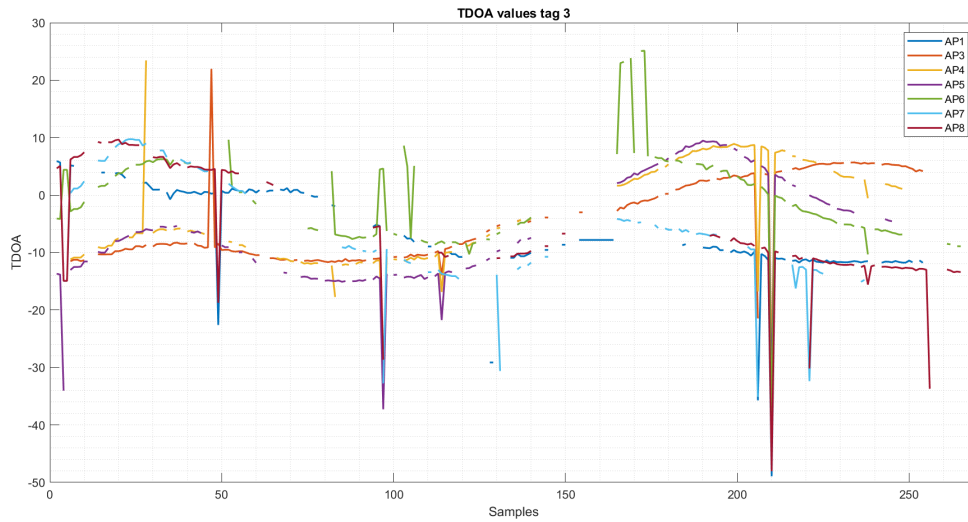
Figure 5.62: Plot of the TDoA measurements evolution, showing the measures for all APs superposed to make the missing parts observed by each device more evident. Results for tag 3
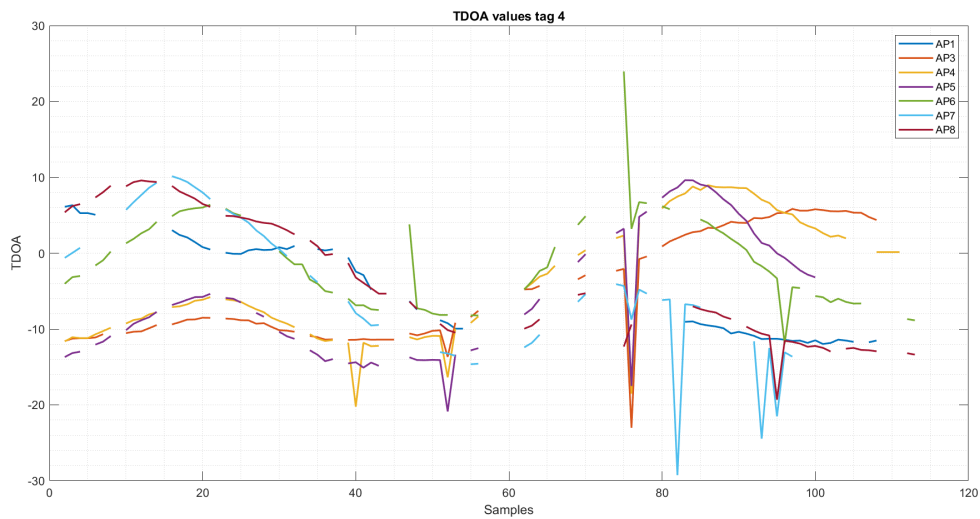
Figure 5.63: Plot of the TDoA measurements evolution, showing the measures for all APs superposed to make the missing parts observed by each device more evident. Results for tag 4
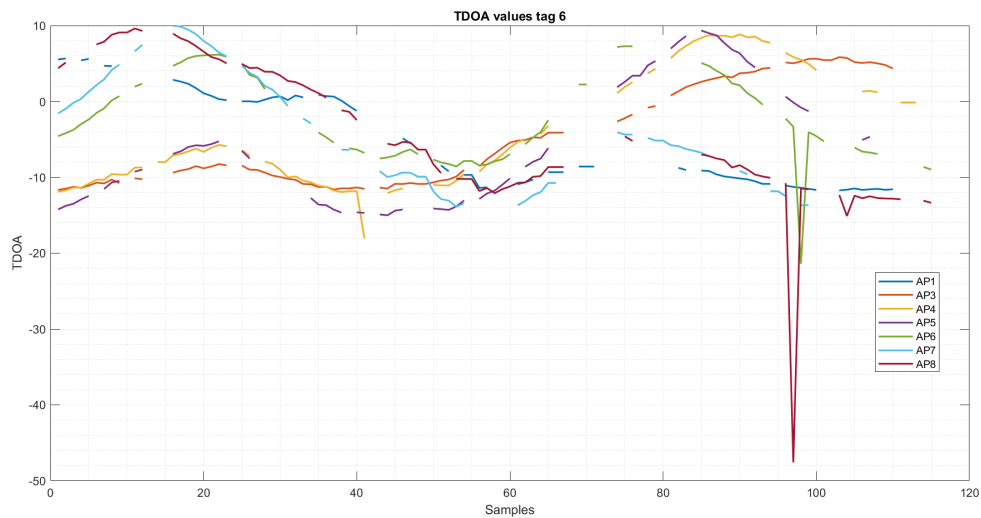
Figure 5.64: Plot of the TDoA measurements evolution, showing the measures for all APs superposed to make the missing parts observed by each device more evident. Results for tag 6
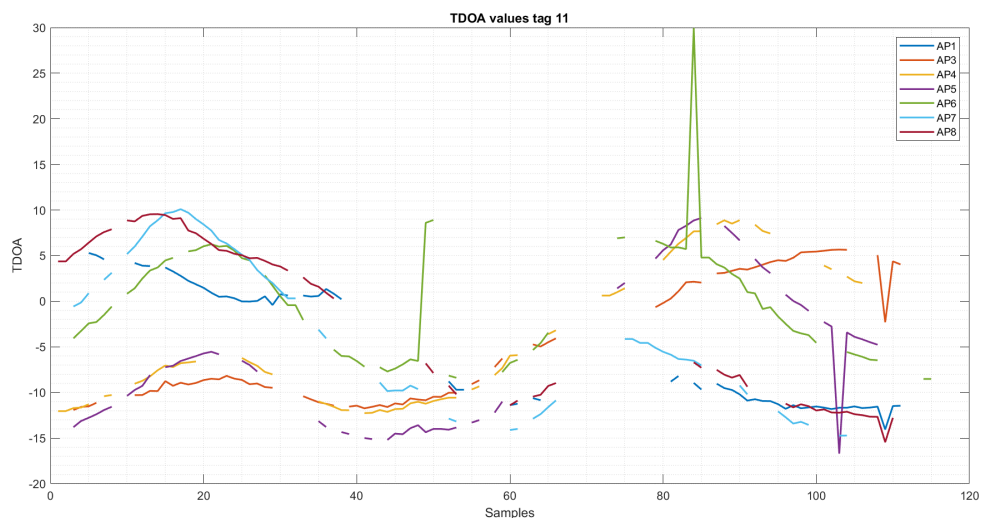
Figure 5.65: Plot of the TDoA measurements evolution, showing the measures for all APs superposed to make the missing parts observed by each device more evident. Results for tag 11

To better highlight the amount of missing data for each anchors, another visual representation is proposed. Figure 5.66, 5.67, 5.68 and 5.69 returns in percentage the number of missing data each anchor. The percentages are reported for each used anchor with respect to all the analyzed tags. A horizontal line is drawn in correspondence to the probability of loosing 30% of the data. To this purpose we can easily see that in most of the case more than 30% of the measurements are lost.
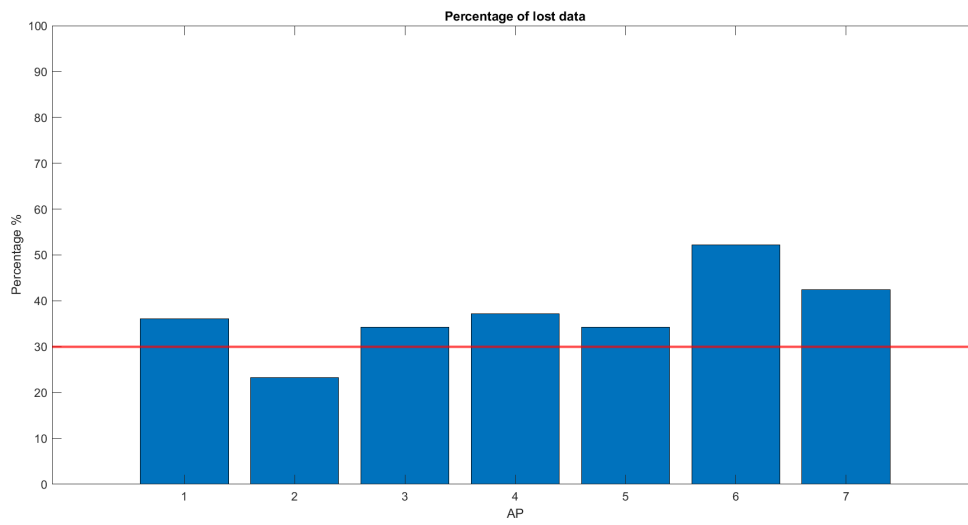
Figure 5.66: Plot of the percentage of lost data for each anchor for tag 3
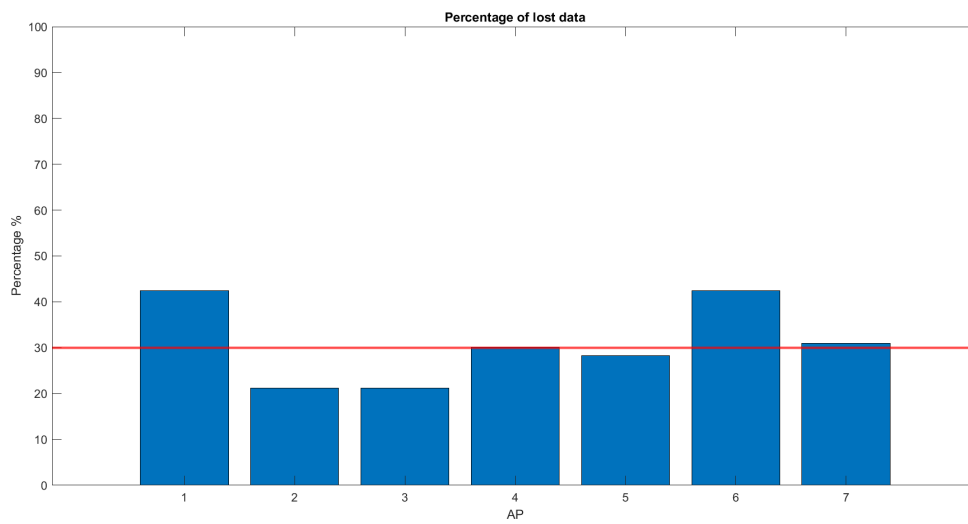
Figure 5.67: Plot of the percentage of lost data for each anchor for tag 4
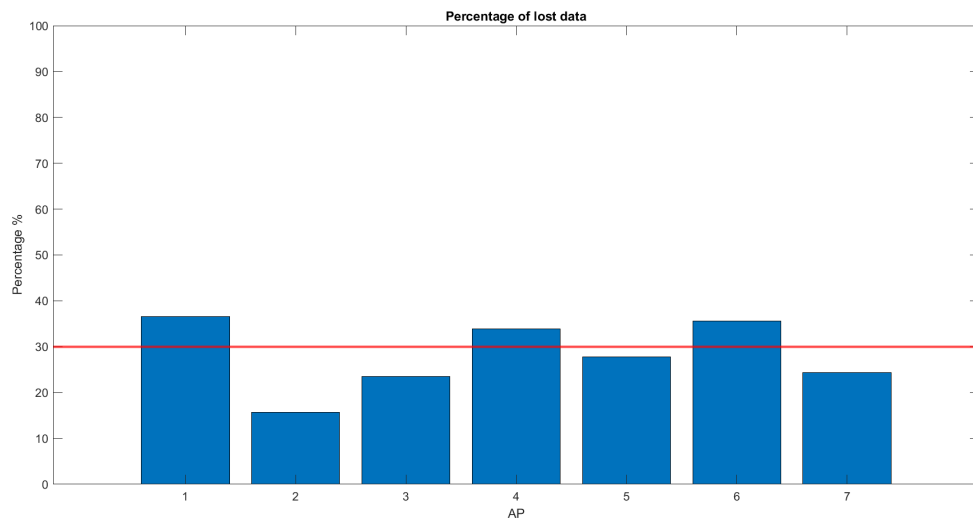
Figure 5.68: Plot of the percentage of lost data for each anchor for tag 6
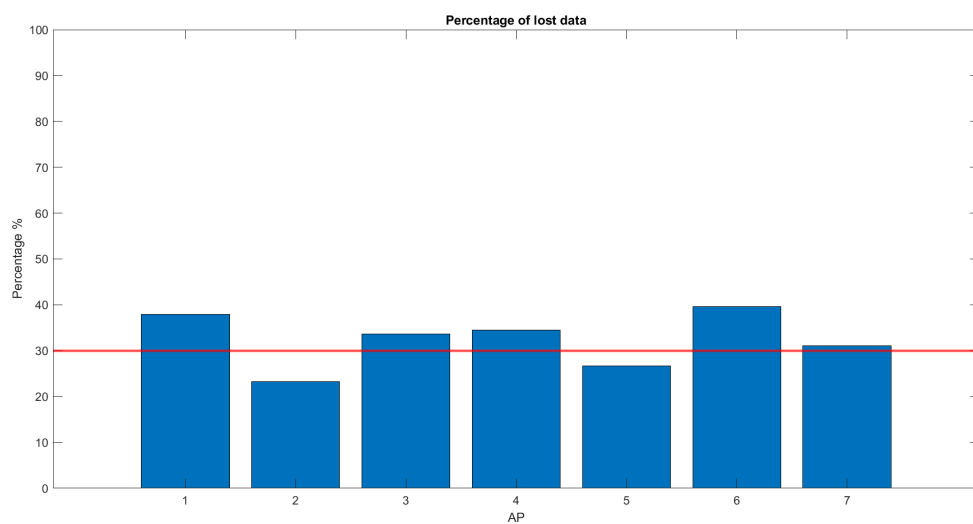
Figure 5.69: Plot of the percentage of lost data for each anchor for tag 11

In conclusion, the utilization of the outdoor acquisition was proven impossible due to data losses related to technical issues connected to the used technology.

6 | Conclusions and future works

The goal of the experimental campaign described in this thesis was to both test and improve the T4F technology for moving targets localization in indoor cluttered environments and compare to the similar character of motion in the outdoor counterpart. The shown results prove that the implementation of a Bayesian tracking filter as the EKF is in fact improving the performance of the system. The UWB technology already allow the overall performance to reach good enough results, but following the movement of a target with precision can only be reached by using an actual tracking method utilizing the obtained data to predict the current position and smoothly draw a correlated path on its visualization output. To install a "plug-and-play" system needs to take into consideration a vast variety of environments in which the system need to properly function. The experimented data also show how, depending on the devices, the system gives in return very different outputs, presenting very noisy ranging measurements which can highly degrade the overall performances and tracking procedure. The devices can improve the performance with the utilization of more efficient inertial systems unit (IMU). The presence of an accelerometer can be used to provide information to the filtering process and improve the localization with a better outlier detection procedure. The acceleration measurement can be used to detect higher position fast changes, consequence of noisy inputs or disturbances to the devices. Implementing a detection algorithm based on the implementation of a new inertial unit can be crucial for the improvement of the overall performance. For what concerns the tracking of human walking targets, a more useful tool can consist in to the use of a gyroscope, to keep track of the person's heading, acting directly on the potential error the tracking filter itself detected on the curves and the positions in which the target was rapidly changing the direction or curving its trajectory. Another solution might consist in the implementation of a system measuring the step length, adding information to the overall sensitivity of the walking features of the target which might change based on the current monitored activity.

Bibliography

[1] Ieee standard for local and metropolitan area networks–part 15.4: Low-rate wireless personal area networks (lr-wpans). *IEEE Std 802.15.4-2011 (Revision of IEEE Std 802.15.4-2006)*, pages 1–314, 2011. doi: 10.1109/IEEESTD.2011.6012487.

[2] B. Denis, L. Ouvry, B. Uguen, and F. Tchoffo-Talom. Advanced bayesian filtering techniques for uwb tracking systems in indoor environments. In *2005 IEEE International Conference on Ultra-Wideband*, pages 6 pp.–, 2005. doi: 10.1109/ICU.2005.1570063.

[3] D. Feng, C. Wang, C. He, Y. Zhuang, and X.-G. Xia. Kalman-filter-based integration of imu and uwb for high-accuracy indoor positioning and navigation. *IEEE Internet of Things Journal*, 7(4):3133–3146, 2020. doi: 10.1109/JIOT.2020.2965115.

[4] V. Fox, J. Hightower, L. Liao, D. Schulz, and G. Borriello. Bayesian filtering for location estimation. *IEEE Pervasive Computing*, 2(3):24–33, 2003. doi: 10.1109/MPRV.2003.1228524.

[5] A. Goldsmith. Wireless communications, 2005.

[6] M. Jassim. The ellipse of position error. *Zanco J. Pure Appl. Sciences.*, pages 24–33, 2019. doi: 10.21271/ZJPAS.31.s3.63.

[7] M. G. K. Meena and A. Kumar. Analysis of uwb indoor and outdoor channel propagation. *IEEE International Women in Engineering (WIE) Conference on Electrical and Computer Engineering (WIECON-ECE)*, 10.1109/WIECON-ECE52138.2020.9397940.:352–355, 2020.

[8] X. R. Li and V. P. Jilkov. Survey of maneuvering target tracking: dynamic models. In *Signal and Data Processing of Small Targets 2000*, 2000. doi: https://doi.org/10.1117/12.391979.

[9] P. M. Ultra-wide band localization system for sport applications. unpublished thesis, 2020.

[10] N. G. M. S. Arulampalam, S. Maskell and T. Clapp. A tutorial on particle filters

for online nonlinear/non-gaussian bayesian tracking,. *IEEE Transactions on Signal Processing*, 50:174–188, 2002.

[11] M. R. Mahfouz, A. E. Fathy, M. J. Kuhn, and Y. Wang. Recent trends and advances in uwb positioning. In *2009 IEEE MTT-S International Microwave Workshop on Wireless Sensing, Local Positioning, and RFID*, pages 1–4, 2009. doi: 10.1109/IMWS2.2009.5307895.

[12] L. Mainetti, L. Patrono, and I. Sergi. A survey on indoor positioning systems. In *2014 22nd International Conference on Software, Telecommunications and Computer Networks (SoftCOM)*, pages 111–120, 2014. doi: 10.1109/SOFTCOM.2014.7039067.

[13] C. Ochoa-Diaz, H. M. Menegaz, A. P. L. Bó, and G. A. Borges. An ekf-based approach for estimating leg stiffness during walking. In *2013 35th Annual International Conference of the IEEE Engineering in Medicine and Biology Society (EMBC)*, pages 7226–7228, 2013. doi: 10.1109/EMBC.2013.6611225.

[14] A. U. Peker, O. Tosun, and T. Acarman. Particle filter vehicle localization and map-matching using map topology. In *2011 IEEE Intelligent Vehicles Symposium (IV)*, pages 248–253, 2011. doi: 10.1109/IVS.2011.5940473.

[15] M. Pham, D. Yang, and W. Sheng. A sensor fusion approach to indoor human localization based on environmental and wearable sensors. *IEEE Transactions on Automation Science and Engineering*, 16(1):339–350, 2019. doi: 10.1109/TASE.2018.2874487.

[16] T. Risset, C. Goursaud, X. Brun, K. Marquet, and F. Meyer. Uwb ranging for rapid movements. In *2018 International Conference on Indoor Positioning and Indoor Navigation (IPIN)*, pages 1–8, 2018. doi: 10.1109/IPIN.2018.8533820.

[17] B. K. S. R. J. C. S. Lee, B. Cho and S. Kim. Kalman filter-based indoor position tracking with self-calibration for rss variation mitigation. *International Journal of Distributed Sensor Networks*, 2015, 2015.

[18] J.-Y. P. Santosh Subedi. Practical fingerprinting localization for indoor positioning system by using beacons. *Journal of Sensors*, 2017:16, 2017.

[19] B. Silva, Z. Pang, J. Åkerberg, J. Neander, and G. Hancke. Experimental study of uwb-based high precision localization for industrial applications. In *2014 IEEE International Conference on Ultra-WideBand (ICUWB)*, pages 280–285, 2014. doi: 10.1109/ICUWB.2014.6958993.

[20] M. Tsogas, A. Polychronopoulos, and A. Amditis. Unscented kalman filter design for

curvilinear motion models suitable for automotive safety applications. In *2005 7th International Conference on Information Fusion*, volume 2, pages 8 pp.–, 2005. doi: 10.1109/ICIF.2005.1592006.

[21] E. A. Wan and R. V. D. Merwe. The unscented kalman filter for nonlinear estimation. pages 153–158, 2000.

[22] M. Švecová and D. Kocur. Localization of a person moving with an unknown character of motion. *Journal of Electromagnetic Waves and Applications*, 35(5):647–671, March 2021. doi: 10.1080/09205071.2020.185.

List of Figures

List of Tables